AD-A174 949 CHEMICAL REACTIONS IN TURBULENT MIXING FLOWS(U) 1/1
CALIFORNIA INST OF TECH PASADENA H W LIEPMANN ET AL.
10 APR 86 AFOSR-TR-86-2122 AFOSR-83-0213
UNCLASSIFIED F/G 20/4 NL

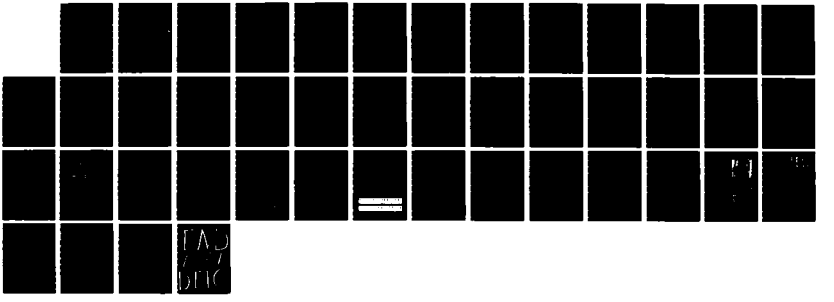

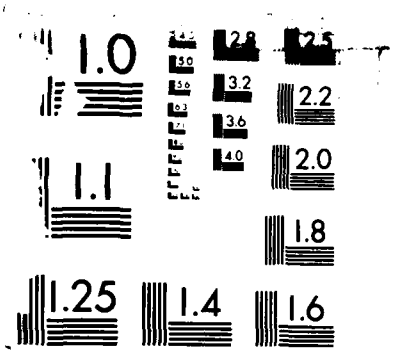


MICROCOPY RESOLUTION TEST CHART

Unclas
SECURITY CL

# AD-A174 949

## DOCUMENTATION PAGE

| | |
|---|---|
| 1a. REPORT SECURITY CLASSIFICATION<br>Unclassified | 1b. RESTRICTIVE MARKINGS<br>None |
| 2a. SECURITY CLASSIFICATION AUTHORITY | 3. DISTRIBUTION/AVAILABILITY OF REPORT<br>Distribution unlimited; approved for public release |
| 2b. DECLASSIFICATION/DOWNGRADING SCHEDULE | |
| 4. PERFORMING ORGANIZATION REPORT NUMBER(S) | 5. MONITORING ORGANIZATION REPORT NUMBER(S)<br>AFOSR-TR- 86-2122 |
| 6a. NAME OF PERFORMING ORGANIZATION<br>California Institute of Technology<br>6b. OFFICE SYMBOL (If applicable) | 7a. NAME OF MONITORING ORGANIZATION<br>Air Force Office of Scientific Research |
| 6c. ADDRESS (City, State and ZIP Code)<br>1201 E. Califor a Blvd.<br>Pasadena, CA 91125 | 7b. ADDRESS (City, State and ZIP Code)<br>Bolling AFB DC 20332-6448 |
| 8a. NAME OF FUNDING/SPONSORING ORGANIZATION<br>Air Force Office of Sciencific Research<br>8b. OFFICE SYMBOL (If applicable)<br>AFOSR/NA | 9. PROCUREMENT INSTRUMENT IDENTIFICATION NUMBER<br>AFOSR-83-0213 |
| 8c. ADDRESS (City, State and ZIP Code)<br>Directorate of Aerospace Sciences<br>Air Force Office of Scientific Research<br>Bolling Air Force Base, DC 20332-6448 | 10. SOURCE OF FUNDING NOS.<br>PROGRAM ELEMENT NO. 61102F; PROJECT NO. 2308; TASK NO. A2; WORK UNIT NO. |
| 11. TITLE (Include Security Classification)<br>"Chemical Reactions in Turbulent Mixing Flows" | |
| 12. PERSONAL AUTHOR(S)<br>H. W. Liepmann, J. E. Broadwell, P. E. Dimotakis | |
| 13a. TYPE OF REPORT<br>~~Interim~~ Annual<br>13b. TIME COVERED FROM _____ TO 4/15/85 | 14. DATE OF REPORT (Yr., Mo., Day)<br>4/10/86<br>15. PAGE COUNT<br>43 |
| 16. SUPPLEMENTARY NOTATION | |

| 17. COSATI CODES | | |
|---|---|---|
| FIELD | GROUP | SUB. GR. |
| 20 | 04 | |
| 21 | 01 | |

18. SUBJECT TERMS (Continue on reverse if necessary and identify by block number)
Turbulence; Flame; Damkohler number; Shear Layer; Jet Combustion

19. ABSTRACT (Continue on reverse if necessary and identify by block number)

Work is continuing in both gas phase and liquid phase turbulent mixing and chemical reactions. In the gas phase shear layer work, our investigations are concentrating on shear layer free stream density ratio effects, finite kinetic rate (Damkohler number) effects, and heat release effects the latter up to a temperature rise in the combustion zone of the order of 1,000 K. In jet flows, the development of laser Rayleigh scattering techniques is progressing towards conserved scalar measurements down to diffusion space and time scales. In the liquid phase work, laser induced fluorescence measurements in both shear layer and jet flows have yielded considerable new information on the mixing process and statistics, permitting direct estimates as the probability density function in both cases. Theoretical work in progress is addressing the finite chemical rate problem as well as the diffusion-limited shear layer mixing problem.

| | |
|---|---|
| 20. DISTRIBUTION/AVAILABILITY OF ABSTRACT<br>UNCLASSIFIED/UNLIMITED ☒ SAME AS RPT. ☐ DTIC USERS ☐ | 21. ABSTRACT SECURITY CLASSIFICATION<br>Unclassified |
| 22a. NAME OF RESPONSIBLE INDIVIDUAL<br>Julian M. Tishkoff | 22b TELEPHONE NUMBER (Include Area Code)<br>(202) 767-4935<br>22c. OFFICE SYMBOL<br>AFOSR/NA |

DD FORM 1473, 83 APR EDITION OF 1 JAN 73 IS OBSOLETE

Unclassified
SECURITY CLASSIFICATION OF THIS PAGE

GRADUATE AERONAUTICAL LABORATORIES
of the
CALIFORNIA INSTITUTE of TECHNOLOGY
Pasadena, California 91125

AFOSR-83-0213 Interim Report

for the Period Ending 15-Apr-85

# CHEMICAL REACTIONS in TURBULENT MIXING FLOWS

Principal investigators:

H. W. LIEPMANN, Professor, Aeronautics

J. E. BROADWELL, Senior Scientist, Aeronautics

P. E. DIMOTAKIS, Professor, Aeronautics & Applied Physics

## ABSTRACT

Work is continuing in both gas phase and liquid phase turbulent mixing and chemical reactions. In the gas phase shear layer work, our investigations are concentrating on shear layer free stream density ratio effects, finite kinetic rate (Damkohler number) effects, and heat release effects the latter up to a temperature rise in the combustion zone of the order of 1,000 K. In jet flows, the development of laser Rayleigh scattering techniques is progressing towards conserved scalar measurements down to diffusion space and time scales. In the liquid phase work, laser induced fluorescence measurements in both shear layer and jet flows have yielded considerable new information on the mixing process and statistics, permitting direct estimates as the probability density function in both cases. Theoretical work in progress is addressing the finite chemical rate problem as well as the diffusion-limited shear layer mixing problem.



A1

## 1.0 INTRODUCTION

Work is continuing in both gas phase and liquid phase turbulent mixing, chemical reactions and combustion. Both experimental and analytical/modeling investigations are in progress, as well as an accompanying effort to develop and augment diagnostic techniques, on an as needed basis, in support of the experimental program.

## 2.0 HF COMBUSTING SHEAR LAYER

### 2.1 Density Ratio Effects

Thee free stream density ratio across the 2-D mixing layer has one of the largest effects on the entrainment and growth of the turbulent region (Dimotakis 1984). Using readily available gases, changes in the growth of the layer by factors of three have been previously reported (Konrad 1976). These results have been confirmed in a few pilot runs at low heat release (Mungal & Dimotakis 1984), but as yet no systematic investigation of this phenomenon has been undertaken.

In particular, we are using the HF shear layer combustion facility to determine how density differences effect chemical reactions, and in the case of high heat release, what effect the existence of three characteristic densities (high speed stream, low speed stream, mixed fluid in the layer) has on both product formation and layer growth. The facility was recently recalibrated for the changes in diluent gases.

### 2.2 Finite Kinetic Effects

An analysis of the effects of finite chemical rates has been carried out for a number of simplified flow geometries. Through this analysis and a model decomposition of the reacting zones within

turbulent shear layer, such as the Broadwell-Breidenthal model, we hope to understand the data already reported, and perhaps predict these effects for flows not yet investigated.

The simplest flow model analysed was the constant entrainment, perfectly mixed region. For this initial value problem, a simple one-step, second order reaction was assumed and the temperature dependance of the rate coefficient was neglected. From this, both an exact solution and a number of special case and asymptotic results have been obtained.

A numerical study of the effects of finite kinetics on a laminar strained diffusion flame has also been performed. In this work, the effects of equivalence ratio, reaction rate, strain rate and activation energy on product distributions have been investigated. In the investigation of high activation energy effects, the hysteresis curve associated with the blow-out and light-up phenomenon has been explored, and the stability of the solutions on this curve has been calculated.

This work is carried out in conjunction with the research described in section 2.5 below.

## 2.3 High Resolution Temperature Sensing Probes

As previously reported, plans to use the 0.6 μm temperature sensing probes have been made and prototypes have been fabricated and tested. The probe mount, support structure and purge/connection block have all been constructed and installed. These probes, however, have a reduced ability to withstand higher dynamic pressures and higher temperatures than our standard 2.5 μm probes. We have decided to defer measurements using these probes, to accommodate the higher temperatures we would like to reach in the near future. See section 2.4 below.

## 2.4 Heat Release Effects

High heat release runs with adiabatic flame temperature rise of up to 940 K are in progress. The previously reported trend of layer thinning is observed to persist. A substantial reduction in overall entrainment of free stream fluid into the layer is caused by heat release. It appears that the reduction in entrainment is more than sufficient to offset the displacement owing to density decrease in the layer by heat release.

An effort is being made to model the effects of heat release on the growth and entrainment of the layer using similarity methods, and it seems that the reported trends of layer thinning and entrainment reduction can be at least partially accounted for by a reduction in the turbulent shear stress by heat release.

Large scale structures are seen to dominate the flow at all levels of heat release. High speed motion picture data were taken over a range of temperatures and are being used to provide statistical information on vortex spacing. Preliminary results suggest a slight reduction in mean vortex spacing with heat release.

Further runs with a favorable pressure gradient were made at an adiabatic flame temperature rise of up to 553 K. For these runs of higher heat release and pressure gradient, the pressure gradient still does not appear to have any significant effect on the amount of mixing and chemical product production in the layer.

A more extensive discussion of these and other results is presented in the appended AIAA Paper 85-0142 by J. C. Hermanson, M. G. Mungal and P. E. Dimotakis, recently presented at the AIAA 23rd Aerospace Sciences Meeting, at Reno, Nevada. This part of the work is nearing completion. A full documentation should be available at the end of the next reporting period (ending April 1986) in the form of a Caltech Ph.D. thesis by J. Hermanson.

## 2.5 Damkohler number - finite rate kinetic effects

The chemical kinetics of the hydrogen/fluorine/nitric oxide system has been studied using the SANDIA (Livermore) CHEMKIN chemical kinetics program. The reactions considered were

$$H_2 + F \rightarrow HF + H \quad (1)$$
$$H + F_2 \rightarrow HF + F \quad (2)$$
$$NO + F_2 \rightarrow NOF + F \quad (3)$$
$$F + NO + M \rightarrow NOF + M \quad (4)$$
$$F + F + M \rightarrow F_2 + M \quad (5)$$
$$H + F + M \rightarrow HF + M \quad (6)$$
$$H + H + M \rightarrow H_2 + M \quad (7)$$

Our nominal concentrations investigated were

$$H_2 = 4\%,$$
$$F_2 = 0.5\%$$

and

$$NO = 0.015\%$$

carried in a nitrogen diluent. The overall chemical reaction time for this system is found to be 0.5 msec.

At our measuring station, the large scale mixing time is 5 msec, based on visual width of the shear layer and the velocity difference. Hence the Damkohler number (ratio of mixing time to chemical time) is 10 when the reaction is mixing limited. This value compares well with that reported earlier by Wallace (1981). The results also show that the overall chemical time is controlled by the NO concentration.

These results are currently being used to interpret the results of our attempts to simulate the effects of slow chemistry. A full

documentation (Broadwell & Mungal) on this part of the work should be available by the end of the next reporting period. The effects of slow chemistry are also important in the context of our long term goals in this program as we would hope to extend the work on chemically reacting flows to supersonic flow speeds, where finite kinetics play an (if not the most) important role.

## 3.0 LIQUID PHASE SHEAR LAYER

Our laser induced fluorescence (LIF) measurements in the water 2-D mixing layer have shown that the initial roll-up of the vortical structures is not symmetric in the transverse dimension of the layer. Results, reported in our earlier progress reports, Koochesfahani P.h. D. thesis 1984 and Koochesfahani & Dimotakis, AIAA paper no. 84-0198, indicate that in the initial roll-up process a large amount of high speed fluid is engulfed into the layer, which then leads into a vortical structure whose core is essentially full of fluid from the high speed stream. The significance of this event is that the composition of the mixed fluid during the mixing transition is not determined solely by the entrainment ratio of fluids from the two free streams into the layer, but also by this initial composition asymmetry in the structure cores as a result of the first roll-up.

There is an effort currently under way to try to understand the initial roll-up process via linear stability theory of the spatially growing disturbances. Our goal is to calculate the geometry of the streakline that peels off the splitter plate which subsequently rolls up into a vortex. The initial set of calculations, using a hyperbolic tangent mean velocity profile at the splitter plate as a test case, agrees with previous results of Michalke (1965). See figure 1. We are now in the process of calculating the streakline for the actual case realized in the laboratory by incorporating the wake of the splitter plate into the mean velocity profile.

## 4.0 SHEAR LAYER MIXING & CHEMICAL REACTIONS MODEL

An analytical model of mixing and chemical reactions, at low heat release, for fully developed, turbulent shear layers has been completed. The model calculates the chemical product thickness ratio $\delta_p/\delta$ (volume fraction of the total width of the shear layer occupied by chemical product), where $\delta_p$ is the product thickness and $\delta$ is the visual thickness of the shear layer. The resulting estimates are a function of the local shear layer Reynolds number $Re = \Delta U \delta/\nu$, Schmidt number $Sc = \nu/D$, and reactant stoichiometric mixture ratio $\phi$. The overall entrainment ratio to the shear layer is an input to the calculation, and is expressed as a function of the velocity and density ratio of the shear layer free streams, using the results of earlier calculations (Dimotakis 1984). The model is essentially without adjustable parameters and assumes that the spectrum of scales of the turbulence contained within the confines of the shear layer edges is described by a Kolmogorov turbulent cascade.

The resulting theoretical estimates for $\delta_p/\delta$, based on this model, are in good agreement with the low heat release data in our HF combustion facility (Mungal & Dimotakis 1984), as well as the liquid phase data of Koochesfahani (1984) at a comparable Reynolds number, successfully accounting for the Schmidt number effect of a factor of approximately 2 between the gas phase and liquid phase data. The model also correctly predicted the Reynolds number dependence of the chemical product in the shear layer, which was recently measured by Mungal, Hermanson & Dimotakis (1984).

## 5.0 TURBULENT JET MIXING & CHEMICAL REACTIONS

### 5.1 Gas Phase Jet Mixing - Laser Rayleigh Scattering

During the past reporting period, the test cell experiments were completed and detailed work was begun on a full scale experiment utilizing Rayleigh scattering techniques. The test cell, which has also been described in our earlier reports, has been used to confirm our performance calculations and provide insight into some of the dynamic characteristics of our Rayleigh scattering system. A schematic of the test cell has been included in figure 2.

The results of the test cell experiments are good. The output voltage from the electronics is linear in the number density of molecules in the focal volume as determined by the test cell pressure. Typical data are given in figure 3. The small scatter in the data is a consequence of the uncertainty in the pressure reading and the mild drift in laser power. Because the gain of the photomultiplier tube is only specified within a factor of 15 by the manufacturer the slope of the line in figure 3 could not be accurately predicted. The signal-to-noise ratio, however, can be predicted since it is a ratio of amplified quantities. Since, in a shot noise limited measurement, the noise voltage increases as the square root of the signal voltage, the noise voltage divided by the square root of the signal voltage should be a constant. This "system" constant, which is related to the signal-to-noise ratio, can be predicted and measured. Since low values of this constant are optimum, figure 4 makes it clear that the predictions fall about twelve percent below the measurements. Which is reasonable agreement since at least 3 or 4 multiplicative factors in the performance calculation can be only be determined within ten percent.

After developing some simple data acquisition software we made some dynamic concentration measurements in the test cell. A transient jet of high cross section gas was introduced through a central orifice above

the focal volume in the test cell. The concentration history was recorded using a portable computer. The results showed that dust particles, whose Mie scattering cross sections are orders of magnitude larger than the molecular Rayleigh cross sections which comprise the signal, can be readily recognized and intelligent signal processing should minimize their effect on the concentration measurements.

The design of a full scale experiment has begun based on the promising results of the test cell work. Laboratory space which has the proper ventilation, gas exhausting capability, and electrical power system is being sought. Some machining has begun of special optical and mechanical components.

This part of the work is co-sponsored by the Gas Research Institute.

## 5.2 Liquid Phase Jet Mixing & Chemical Reactions

Our work on entrainment, mixing and chemical reaction in high Schmidt number (liquid phase) turbulent jets has continued.

We have completed direct measurements of concentration using LIF digital imaging simultaneously at 1024 points along the jet axis. These measurements have yielded axial PDFs of jet fluid concentration, and have revealed a similarity concentration in terms of which the PDFs in the jet display self-similarity along any ray ( $r/x$ = constant ). This self-similarity permits the cross-over from near-field to far-field jet mixing to be defined quantitatively, and allows the self-similar form of the PDF throughout the jet far-field to be determined without the resolution limitations inherent in any direct measurement.

We have also completed similar imaging measurements of instantaneous radial concentration profiles across the jet in the far field (see Dahm & Dimotakis 1985, appended). These results demonstrate

quantitatively that instantaneous profiles of concentration do not resemble the mean concentration profile. Specifically, the mixed fluid within large regions in the jet usually lies within a narrow range of values, and unmixed ambient fluid can be found throughout the jet. The mean profile is, therefore, a poor representation of the mixed fluid states within the jet. This contrasts with the classical picture of jet mixing, and may have particularly important implications for the modeling of jet mixing and the prediction of chemical reactions between the mixed and ambient entrained fluid.

A full documentation of this effort should be available in the next reporting period (ending 15-Apr-86) in the form of a Caltech Ph.D. thesis by W. Dahm.

This part of the work is co-sponsored by the Gas Research Institute.

## 5.3 Laser Soot Scattering in Jets and Buoyant Flames

A novel combustion diagnostic technique is being explored which makes use of laser light scattering from soot particles in a flame. While many laser-based diagnostics are limited by the presence of soot, the soot particles themselves can in fact be utilized as an important marker within the flame. The submicron particles are strong scatterers of visible radiation (relative to molecular scattering cross-sections) and by directing the intense, monochromatic beam of a laser through the soot distribution (flame), the location of soot along the line of the beam can be determined. The essence of this new technique is to measure the intensity of the soot scattering along a specified line segment in the flame as a function of time.

Photodiode array and computer data acquisition technology for measuring and recording such an intensity pattern has been developed and extensively used in our laboratories. Its application in a soot

scattering experiment is straightforward. Some preliminary feasibility studies using a 3 watt argon-ion laser and a buoyant, sooting flame indicated that, by visual inspection, measurable scattered light appears to be present. Although flame luminosity could be expected to interfere with such a measurement, the very narrow line width of the laser combined with a narrow band optical filter greatly diminishes this problem. This technique should contribute to a variety of combustion studies, potentially addressing such questions as flame structure, combustion zone location and character, and the process of sooting.

In order to make more quantitative measurements and to get some idea of the type of information that can be gained with such a technique, an optical system was designed. The purpose of the optical system is to pass the laser beam through the flame in an easily controlled manner and to collect only the scattered laser light, discriminating against the unwanted flame luminosity. With this apparatus, several sets of photographs of the buoyant methane flame above a 50 cm diameter glass-bead burner were taken. These photographs verify our initial estimates of the technique's efficacy and provide a few insights into the soot distribution patterns within the flame.

These photographs indicate that scattered radiation is always closely associated with a specific intersection of the luminous soot distribution with the laser beam. We saw no evidence of appreciable laser scattering from any region where there was no luminosity. In other words, we saw no appreciable cold soot far from a flame sheet. In this sense, the soot can be considered as approximately marking parts of the flame sheet surface.

Perhaps even more striking was the observation that the soot fills a very small fraction of the total volume of the flame. When the soot distribution intersects the laser beam segment, it showed up as a few small points along the segment, occasionally appearing as a short length much shorter that the width of the overall flame. These observations are consistent with a very convoluted flame sheet that has been strained

out (at least as far as soot production is concerned) at some regions in its topology and which intersects the segment under study at only a few points or occasionally as a short segment when the angle of intersection is quite oblique.

We are presently working on implementing the photodiode array to image the segment, using the same beam steering and collection optics. By interfacing the array to a computer data acquisition system with high speed A/D conversion, we will record the soot distribution along the imaged segment as a function of time. This will give us a more complete picture of the structure of the soot distribution and the flame sheet.

This part of the work is co-sponsored by the Gas Research Institute.

## 6.0 References

DAHM, W. J. A. and DIMOTAKIS, P. E. [1985] "Measurements of Entrainment and Mixing in Turbulent Jets", AIAA 23rd Aerospace Sciences Meeting 14-17 January 1985 (Reno, Nevada), AIAA Paper No. 85-0056.

DIMOTAKIS, P. E. [1984] "Entrainment into a Fully Developed, Two-Dimensional Shear Layer", AIAA 22nd Aerospace Sciences Meeting (Reno, Nevada), AIAA Paper No. 84-0368.

HERMANSON, J. C., MUNGAL, M. G. and DIMOTAKIS, P. E. [1985] "Heat Release Effects on Shear Layer Growth and Entrainment", AIAA 23rd Aerospace Sciences Meeting 14-17 January 1985 (Reno, Nevada), AIAA Paper No. 85-0142.

KONRAD, J. H. [1976] An Experimental Investigation of Mixing in Two-Dimensional Turbulent Shear Flows with Applications to Diffusion-Limited Chemical Reactions, Ph.D. Thesis, California Institute of Technology, and Project SQUID Technical Report CIT-8-PU (December 1976).

KOOCHESFAHANI, M. M. [1984] Experiments on Turbulent Mixing and Chemical Reactions in a Liquid Mixing Layer, Ph. D. thesis, California Institute of Technology.

KOOCHESFAHANI, M. M. and DIMOTAKIS, P. E. [1985] "Laser Induced Fluorescence Measurements Concentration in a Plane Mixing Layer", AIAA 22nd Aerospace Sciences Meeting (Reno, Nevada), AIAA Paper No. 84-0198, published in the AIAA J. 23(11), 1700-1707.

MICHALKE, A. [1965] "On spatially growing disturbances in an inviscid shear layer", J. Fluid Mech. 23(3), 521-544.

MUNGAL, M. G. and DIMOTAKIS, P. E. [1984] "Mixing and combustion with low heat release in a turbulent mixing layer", J. Fluid Mech. 148, 349-382.

MUNGAL, M. G, HERMANSON, J. C. and DIMOTAKIS, P. E. [1985] "Reynolds Number Effects on Mixing and Combustion in a Reacting Shear Layer", AIAA J. 23(9), 1418-1423.

WALLACE, A. K. [1981] Experimental Investigation on the Effects of Chemical Heat Release in the Reacting Turbulent Plane Shear Layer, Ph. D. thesis, University of Adelaide, also distributed as AFOSR-TR-84-0650.

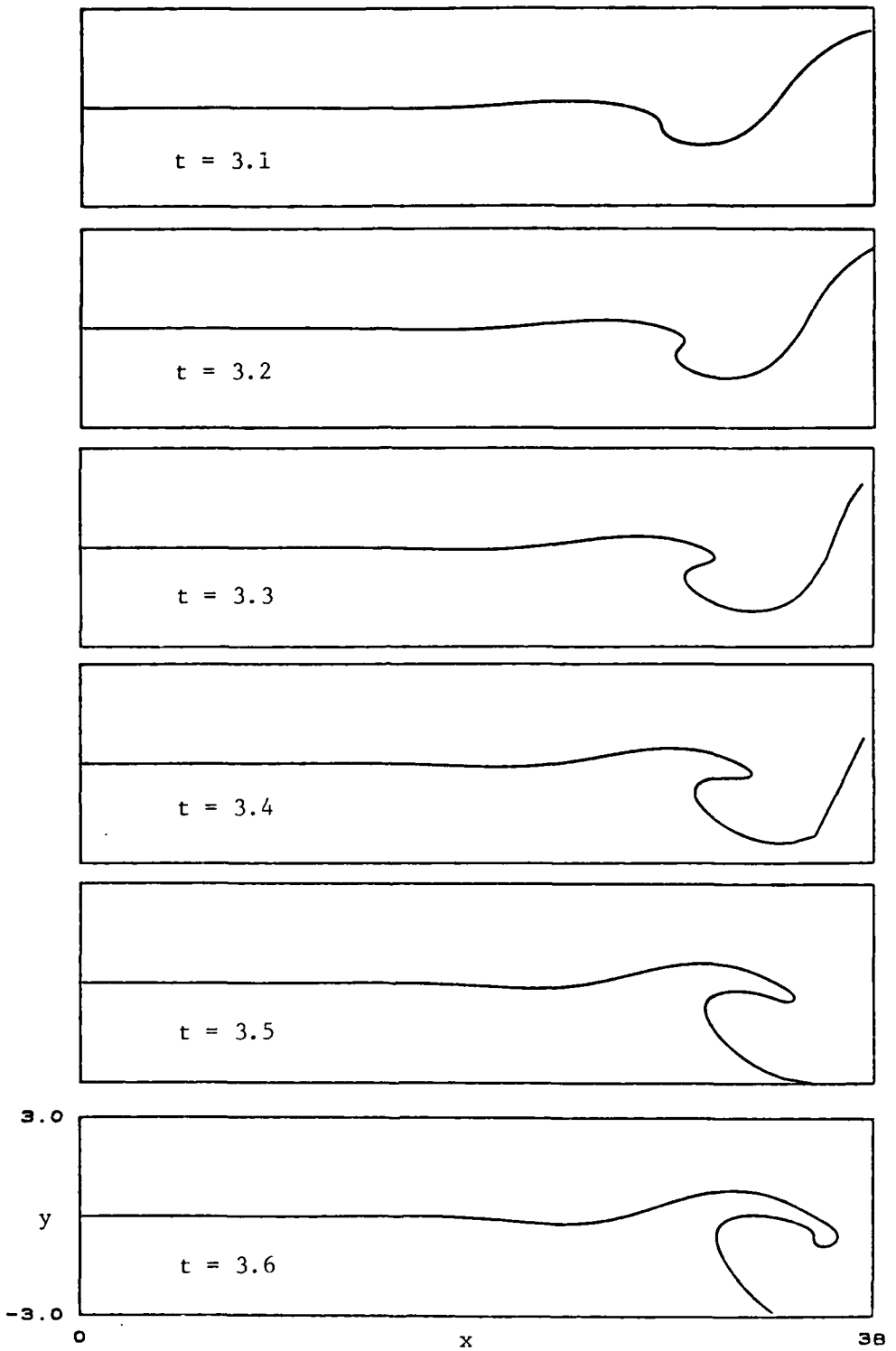


Roll-up of the streak line for the hyperbolic-tangent velocity profile calculated for the most amplified frequency.

Figure 1

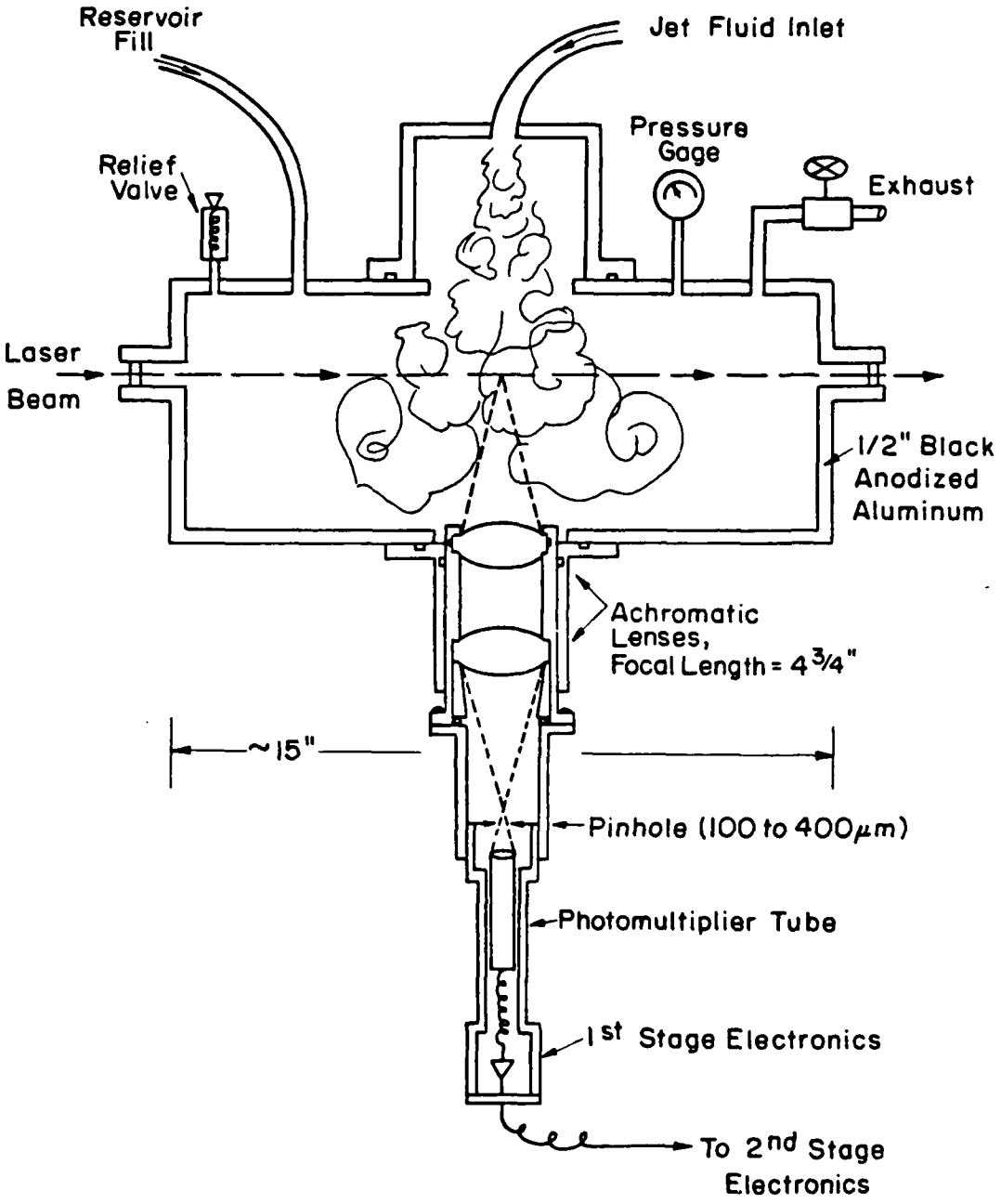


RAYLEIGH SCATTERING TEST CELL SCHEMATIC

Figure 2

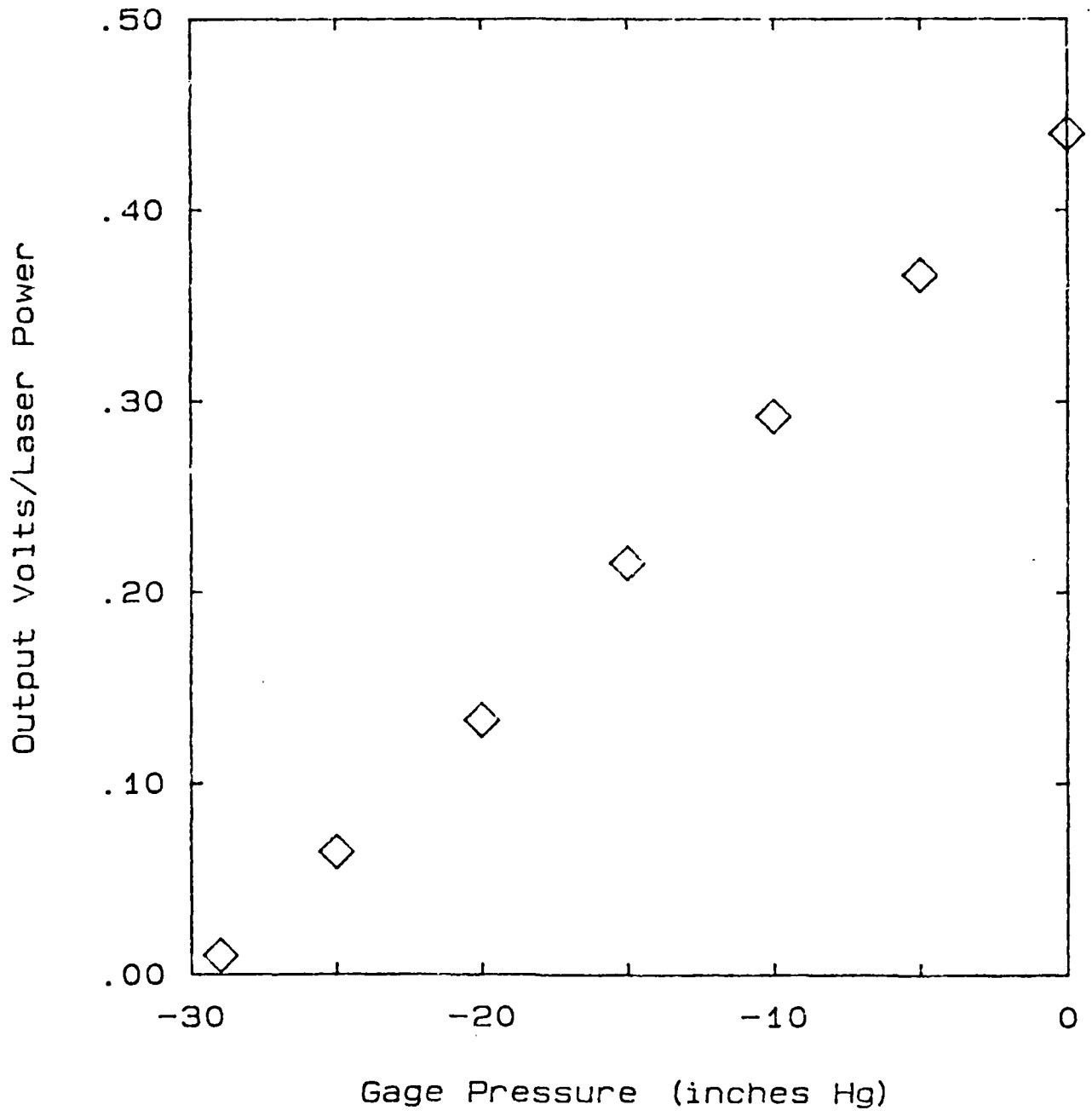
.50
.40
.30
.20
.10
.00
Output Volts/Laser Power
-30
-20
-10
0
Gage Pressure (inches Hg)

Figure 3

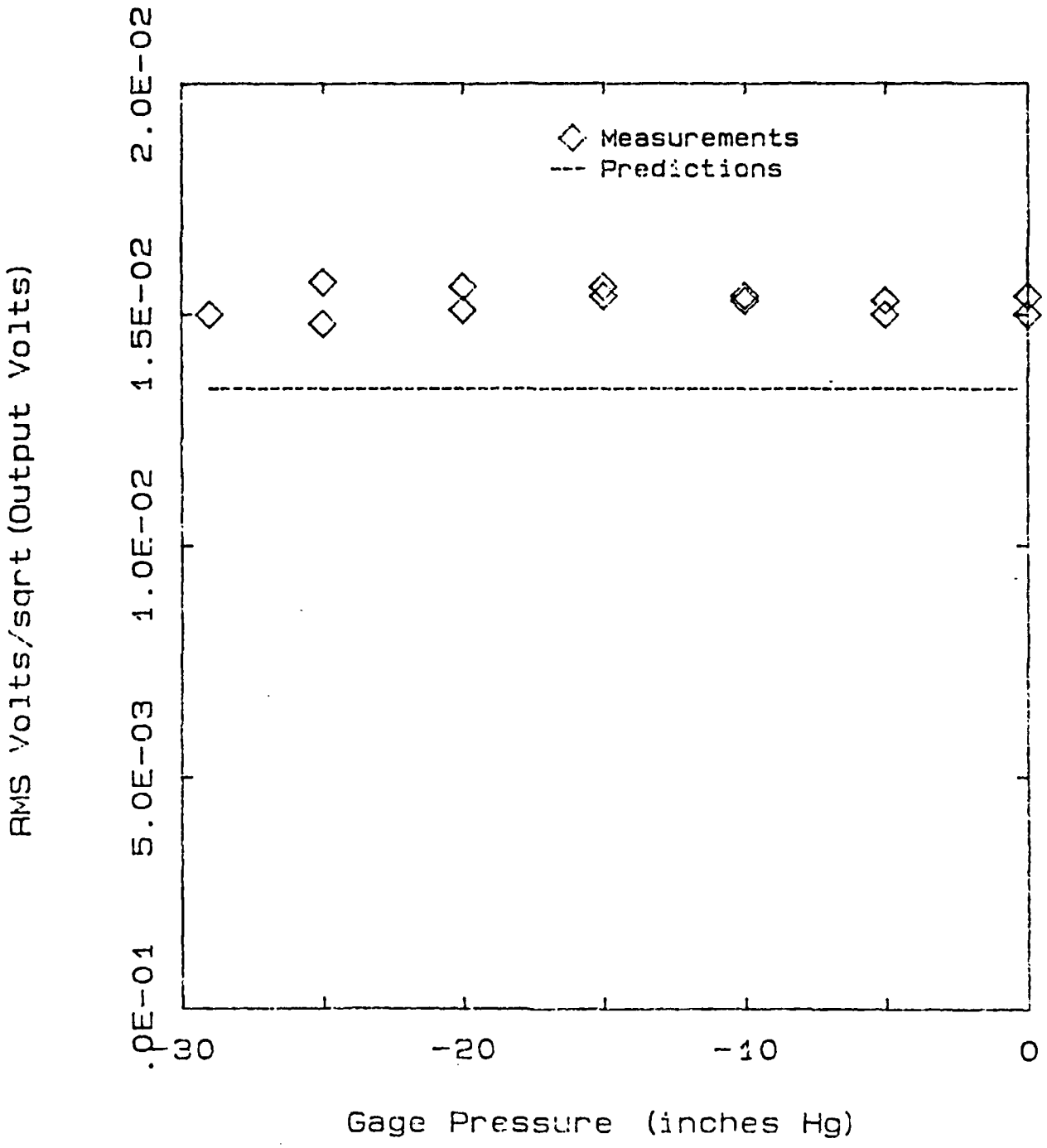
RMS Volts/sqrt(Output Volts)
2.0E-02
1.5E-02
1.0E-02
5.0E-03
.0E-01
Measurements
Predictions
-30
-20
-10
0
Gage Pressure (inches Hg)

Figure 4

AIAA'85

AIAA-85-0142

# Heat Release Effects on Shear Layer Growth and Entrainment

J.C. Hermanson, M.G. Mungal,
P.E. Dimotakis

California Institute of Technology
Pasadena, CA.

**AIAA 23rd Aerospace Sciences Meeting**

January 14-17, 1985/Reno, Nevada

# HEAT RELEASE EFFECTS ON SHEAR LAYER GROWTH AND ENTRAINMENT

J. C. Hermanson* , M. G. Mungal+ and P. E. Dimotakis#
California Institute of Technology
Pasadena, California

## ABSTRACT

The effects of heat release are studied in a planar, gaseous reacting mixing layer formed between free streams containing hydrogen and fluorine in inert diluents. Sufficiently high concentrations of reactants are employed to produce adiabatic flame temperature rises of up to 940 K (1240 K absolute). Though the displacement thickness of the layer, for zero streamwise pressure gradient, increases with increasing heat release, the actual thickness of the mixing layer is not observed to increase, and is in fact characterized by a slight thinning. The overall entrainment into the layer is seen to be substantially reduced by heat release. The large scale vortical nature of the flow appears to persist at high temperatures. Imposition of a favorable pressure gradient, though resulting in additional thinning of the layer, is observed to have no resolvable effect on the mixing and amount of chemical product formation.

## INTRODUCTION

This investigation is concerned with heat release effects in a gas phase turbulent, plane, reacting shear layer at high Reynolds number. The work is an extension of earlier work in the same facility[19,20,21]. The flow consists of a two-dimensional mixing layer with gas phase free streams, one stream carrying a given concentration of hydrogen in an inert diluent; the other, fluorine. The reaction $H_2 + F_2 \rightarrow 2\,HF$ is highly exothermic so that reactant concentrations of 1% $H_2$ and 1% $F_2$ in an $N_2$ diluent respectively produce an adiabatic flame temperature rise of 93 K above ambient. Results will be presented here corresponding to fluorine concentrations of up to 6% and hydrogen concentrations of up to 24%, with a maximum adiabatic flame temperature rise of 940 K (corresponding to 1240 K absolute).

In earlier work by Mungal et al[19,20,21], with temperature rises of up to 165 K, no coupling of heat release with the fluid mechanics could be observed, as manifested by the growth rate, entrainment and discernible large scale structure dynamics. In that work, the chemical reaction could be considered as a diagnostic to infer the amount of molecular mixing without disturbing the overall properties of the layer. In the work reported here, the heat release is much larger and the effects of the heat release itself on the properties of the shear layer are investigated. The highest heat release cases reported here are sufficiently hot to result in a mean density reduction in the center of the layer of about 65%.

## EXPERIMENTAL FACILITY AND INSTRUMENTATION

The experimental apparatus is described in detail in Mungal et al[20]. It is a blowdown facility in which premixed volumes of fluorine in an inert diluent and hydrogen in an inert diluent are discharged through sonic orifices to maintain a constant mass flux. Each stream enters a settling and contraction section for turbulence suppression with the high speed stream emerging from a 6:1 contraction with an exit area of 5 x 20 cm, and the low speed emerging from a 4:1 contraction in a 7.5 x 20 cm exit area. The two streams meet at the tip of a splitter plate, with a trailing edge included angle of 3.78°. The high speed free stream turbulence level was measured to be about 2/3%.

To offset the free stream density difference that results from large amounts of hydrogen in one stream, the densities of the free streams were matched for most cases by using as diluent a mixture of nitrogen and a small amount of helium, on the fluorine side, and a mixture of nitrogen with a small amount of argon on the hydrogen side. The intent was also to match the heat capacities of the two free streams.

Runs were performed with a nominal high speed flow velocity of 22 m/s, and a free stream speed ratio of $U_2/U_1 = 0.4$. In practice, these values varied slightly -- a result of differences in gas constants of the various mixtures -- although the sonic metering orifices were adjusted for each run

* Graduate Student, Aeronautics. Member AIAA.
+ Research Fellow, Aeronautics. Member AIAA
# Associate Professor, Aeronautics and Applied Physics. Member AIAA.

to minimize these variations. The measuring station was positioned 45.7 cm downstream of the splitter plate trailing edge. The Reynolds number at the measuring station was typically $Re_{\delta_1} = 6 \times 10^4$, based on the free stream velocity difference, the 1% thickness of the mean temperature profile, and the cold free stream kinematic viscosity. The 1% thickness, $\delta_1$, of the temperature or concentration field [18,20], is defined here as the transverse width of the layer at which the mean temperature rise is 1% of the maximum mean temperature rise and has been shown[20] to correlate well with the visual thickness $\delta_{vis}$ (Brown & Roshko[8]) of the layer. This value of the Reynolds number is well above that for the mixing transition as reported by Bernal et al[3], Breidenthal[6] and Konrad[17]. The corresponding Reynolds number based on the high speed free stream velocity and on the downstream distance was $Re_x = 6 \times 10^5$. A diagram of the shear layer geometry is shown in Figure 1.

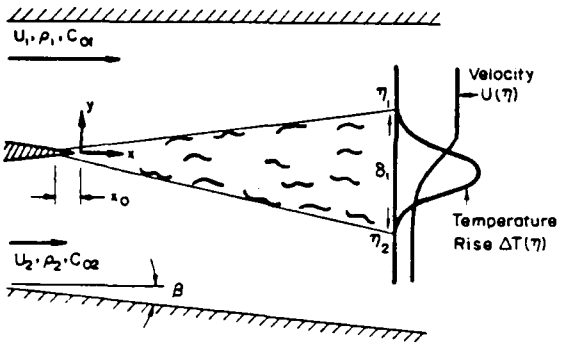


Fig. 1 Turbulent Shear Layer Geometry

Temperature data were recorded with a rake of eight 2.5 μm diameter platinum - 10% rhodium cold wires, with a typical wire span of 1.5 mm, welded to Inconel prongs. For some runs a rake of 25 μm diameter Chromel-Alumel thermocouples was employed. It was found that the 2.5 μm resistance wires in the hottest regions did not survive in runs in which the adiabatic flame temperature rise exceeded approximately 600 K. Both the cold wire and thermocouple rakes were positioned across the transverse extent of the layer. The total data rate for the resistance wires was 80 kHz, corresponding to 10 kHz per probe. The thermocouples were sampled at 500 Hz each, for a total data rate of 4 kHz; their considerably lower frequency response not warranting a higher rate.

Thermocouples produce a voltage proportional to the junction temperature and normally do not require calibration. The resistance wires were calibrated as described previously[19] using a hot and cold jet of known temperature. The two measurements provided calibration constants to convert voltage to temperature rise. An additional correction was applied to the output signal voltage in the present experiments to account for the non-linearity in the resistivity of the platinum - 10% rhodium wire element at elevated temperatures[10]. It was determined that for neither the thermocouples nor the resistance wires was there significant radiation error for the temperatures in this investigation[24]. Both probes, however, are influenced by heat conduction to the support prongs, which can result in excursions from the mean temperature being in error by as much as 10% to 20% for the cold wires and up to 40% for the thermocouples. Both diagnostics, however, produce accurate mean temperatures, as during a small fraction of the course of the run (before data acquisition begins) the tips of the support prongs assume the local mean value. Good agreement (typically within 5%) was obtained during runs in which both sets of probes were employed. Errors resulting from differences in the thermal conductivity of the fluid from each of the free streams were established to be small.

In addition to the temperature data, a schlieren system was utilized for concurrent flow visualization. The beam width utilized was sufficient to illuminate 25 cm of the shear layer. A circular source mask and a circular hole spatial filter were used in place of the conventional source slit and knife edge in an effort to give equal weights to gradients in index of refraction in all directions and better resolve the large scale structure of the flow. The hole sizes were increased with increasing flow temperature to optimize (reduce) sensitivity as needed. High time resolution spark schlieren photographs were taken with a spark source (~ 3 μsec duration), synchronized with a motor-driven 35 mm camera, at a rate of approximately three frames per second.

The mean velocity profile was measured for most runs by a pitot probe rake of fifteen probes connected to a miniature manometer bank filled with fluorine resistant oil (Hooker Chemical

Fluorolube FS-5) with an adequate time response to yield a reliable mean dynamic pressure profile during each run. The bank was photographed by a second motor-driven 35 mm camera. The photographic data were digitized and reduced to mean velocity profiles. This technique of measuring the pitot pressure was estimated to be accurate to 5%. Rebollo[23] estimated that the accuracy of extracting mean velocities from pitot pressures in non-constant density flows is about 4-5%.

Finally, the streamwise static pressure gradient was monitored by measuring the pressure difference between two downstream locations on the low speed sidewall with a Datametrics type 573 fluorine resistant Barocel sensor. The high speed side wall was kept horizontal for all runs and the low speed side wall was adjusted for the desired streamwise pressure gradient. The wedge-like geometry of the planar shear layer displacement allows this simple means of accommodating or imposing any desired pressure gradient. Most of the runs in the present investigation were performed with the sidewalls adjusted to the requisite divergence angle to ensure a zero streamwise pressure gradient. For some runs at high heat release, the walls were left fixed at the angle required for zero pressure gradient at zero heat release, which allowed the heat release to induce a favorable streamwise pressure gradient (accelerating flow), as a result of the combustion displacement effects.

## CHEMISTRY

The chemical reaction utilized in the present investigation is effectively

$$H_2 + F_2 \rightarrow 2HF \ , \quad \Delta Q = -130 \text{ kcal/mole}$$

This yields a temperature rise of 93 K for 1% $F_2$ and 1% $H_2$ in $N_2$ diluent under constant pressure, adiabatic conditions (this is the so-called adiabatic flame temperature rise). The chemical reaction actually consists of two second order chain reactions:

$$H_2 + F \rightarrow HF + H, \quad \Delta Q = -32 \text{ kcal/mole}$$

$$H + F_2 \rightarrow HF + F, \quad \Delta Q = -98 \text{ kcal/mole}$$

Proper chain initiation requires some free F atoms, which were generated in these experiments by premixing a trace amount of nitric oxide into the hydrogen-carrying stream. This allows the reaction

$$F_2 + NO \rightarrow NOF + F$$

which provides the required small F atom concentration in the layer to sustain proper ignition. For all runs in this investigation, the NO concentration was maintained at 3% of the free stream fluorine concentration.

For all flows reported here, the resulting chemical time scales are fast compared with the fluid mechanical time scales. The chemical time scales for the reaction, over the entire range of concentrations, were determined using the CHEMKIN chemical kinetics program[15]. The chemical rate data for the reactions involved were taken from Cohen & Bott[11] and Baulch et al[2]. The Dahmköhler number (ratio of mixing time to chemical time) based on the local, large scale characteristic time ($\delta_1 / \Delta U$, where $\Delta U$ is the free stream velocity difference) ranges from 25 to 125 with increasing reactant concentrations. The Dahmköhler number based on the time of flight from the splitter tip to the measuring station ($x / U_c$, where $U_c$ is the large structure convection velocity) varies from 160 to 800. For comparison, the Dahmköhler numbers for the low heat release work of Mungal[19,20,21] were 10 and 60 for the large scales and time of flight, respectively. In those investigations, the chemistry was shown to be already fast. Chemical kinetics are, consequently, not an issue in the present investigation, where the chemistry is much faster as a result of the higher reactant concentrations and combustion temperatures.

The equivalence ratio, $\phi$, is defined here as the volume of high speed fluid required to completely react with a unit volume of low speed fluid. This is the same as the ratio of the low speed free stream molar concentration, $c_{02}$, to the high speed free stream molar concentration, $c_{01}$, divided by the low speed to high speed stoichiometric ratio, i.e.

$$\phi = \frac{c_{02}/c_{01}}{(c_{02}/c_{01})_s} = c_{02}/c_{01}$$

In this case, since the molar stoichiometric ratio for the hydrogen-fluorine reaction is unity.

## RESULTS AND DISCUSSION

### I. Growth Rate and Entrainment

The low speed sidewall divergence required for zero streamwise pressure gradient is a direct measure of the displacement thickness of the layer, $\delta^*$, where $\delta^*/x$ indicates the tangent of the angle by which the low speed free streamline is shifted owing to the presence of the shear layer. Note that the displacement thickness is less than zero for a layer with no heat release, and increases steadily with heat release, as shown in Figure 2. The parameter $(\rho_0 - \bar{\rho})/\rho_0$ represents the mean normalized density reduction in the layer due to heat release, where $\bar{\rho}$ is the mean density in the layer and $\rho_0$ is the average (cold) density of the free streams.

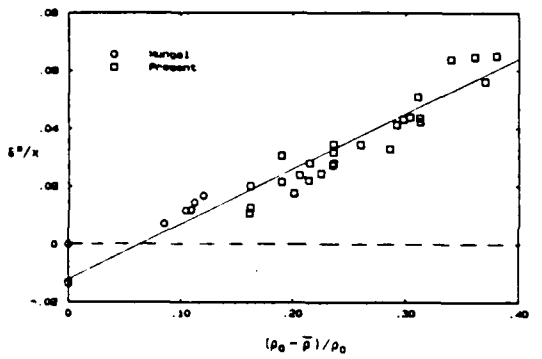


Fig. 2 Layer Displacement due to Heat Release

It may be worth noting that the actual shear layer thickness ($\delta_1$ or $\delta_{vis}$), in spite of large heat release and large density changes, does not increase and, in fact, shows a slight decrease, even though the displacement thickness increases with heat release. This effect was noted by Wallace[26] and is observed in the present set of experiments, in which the maximum mean flow temperature increase is about three times greater than that of Wallace. The observed 1% temperature profile thickness at zero pressure gradient is plotted versus the mean density in the layer in Figure 3. Since it is difficult to hold the speed ratio at exactly 0.40 from run to run and also because the density ratio of the free streams is slightly different from unity for some runs, each data point has been corrected by normalization with the expected growth rate for a cold layer with the identical speed and density ratio, using a formula derived in Dimotakis[12]. A straight line least squares fit to the data suggests that the thinning, for a mean density reduction of 40%, may be as high as 15%. No dependence of the thinning trend on equivalence ratio was observed.

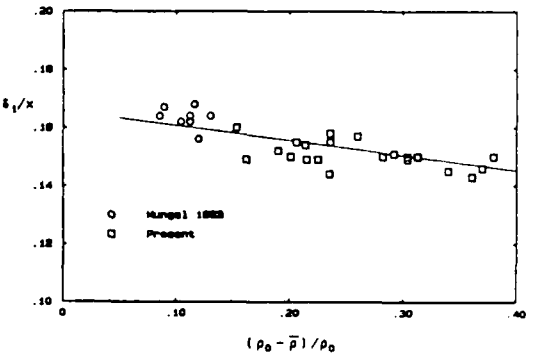


Fig. 3 Layer Thinning with Heat Release

The slight reduction in layer thickness with increasing heat release is confirmed by the mean velocity data. Sample velocity profiles, at different heat release but identical speed and density ratios, are presented in Figure 4. It can be seen that the hotter layer is noticeably steeper in maximum slope, in agreement with

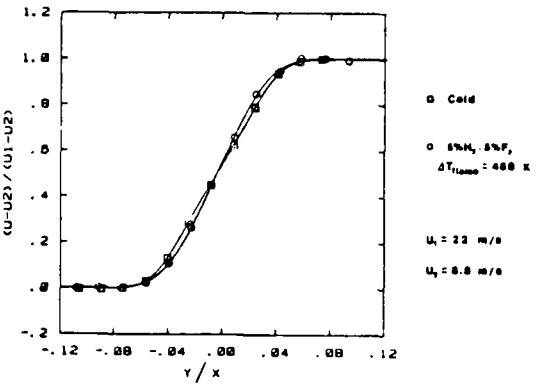


Fig. 4 Effect of Heat Release on Shear Layer Mean Velocity Profile

Wallace[26]. Normalization of this maximum slope by the free stream velocity difference gives the vorticity thickness $\delta_\omega$ of the layer,

$$\frac{1}{\delta_\omega} = \frac{1}{\Delta U}\left(\frac{dU}{dy}\right)_{max} .$$

A plot of the vorticity thickness variation with heat release, again corrected for variations in speed ratio and density ratio, is shown in Figure 5. Each point is normalized by the corresponding cold flow vorticity thickness. The portion of the present results at moderate heat release, including some of the unpublished data of Mungal, are seen to be in good agreement with Wallace[26]. The abscissa parameter of Figure 5, $\bar{\theta}_{max} = \overline{\Delta T}_{max}/T_0$, the maximum mean temperature rise over the ambient temperature, scales differently than $(\rho_0 - \bar{\rho})/\rho_0$, the normalized mean density reduction, and renders the thinning effect at lower temperatures more apparent.

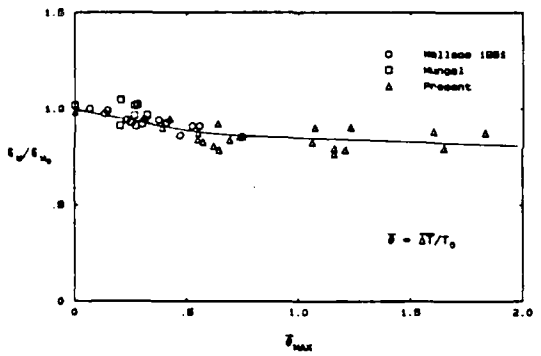


Fig. 5 Effect of Heat Release on Vorticity Thickness

An investigation, at higher temperatures, by Pitz & Daily[22] in a combusting mixing layer formed downstream of a rearward facing step found that the vorticity thickness did not appear to change between their cold runs and high heat release runs. Keller & Daily[16], however, report that in a reacting mixing layer between a cold premixed reactant stream and a preheated combustion product stream, the vorticity thickness increases significantly with increasing temperature. The reasons for the discrepancy between these results and the ones reported here are not clear at this writing.

A complicating factor in any discussion of growth rate is the location of the virtual origin, $x_0$, since the relevant similarity downstream coordinate is in fact $y/(x - x_0)$. The trends in layer thinning reported here do allow the possibility that some of the effects could be accounted for by a shift in the virtual origin with heat release. The changes in $x_0$ with heat release have not been investigated as yet. That initial conditions can have a significant effect on layer growth has been shown, for example, by Browand & Latigo[7]. See also Batt[1], Bradshaw[4] and the discussion in the review paper by Ho & Huerre[14].

One implication of the fact that the layer width does not increase with increasing temperature is that, since the density in the layer is substantially reduced but the layer does not grow faster, the volumetric entrainment of free stream fluid into the layer must also be greatly reduced by heat release. The amount of entrainment into the layer can be calculated from the mean velocity and density (i.e. temperature) profiles as follows:

$$\frac{\dot{V}}{U_1 x} = \int_{\eta_2}^{\eta_1} \frac{\rho U}{\rho_0 U_1} d\eta ,$$

where $\dot{V}$ is the volume flux into the layer per unit span, $x$ is the downstream coordinate, and $\eta = y/x$ is the shear layer similarity coordinate. This expression assumes that the layer is self-similar at the station at which the integral is performed. The quantity $\rho U$ was computed as $\bar{\rho}\,\bar{U}$, which was used here as an approximation for the density-velocity correlation $\overline{\rho U}$.

Results from Mungal et al[21] suggest that there is a Reynolds number dependence on product formation. Since the growth rate does appear to be a function of the product formation (i.e. heat release), strictly speaking, the flow would not be expected to be exactly self similar. An alternate method[9,12] which approximates the overall entrainment is to use the geometry of the layer as shown in Figure 1 to derive:

$$\frac{\dot{V}}{U_1 x} = \eta_1 - r(\eta_2 + \tan\beta) ,$$

where $r = U_2/U_1$, $\eta_{1,2}$ are the similarity coordinate edges of the shear layer, and $\beta$ is the deflection angle of the low speed side wall. A common difficulty of both methods is that of selecting the proper values for $\eta_1$ and $\eta_2$. One reasonable choice is the pair of points corresponding to the 1% edges of the temperature

profile. Resulting calculations for choices of 1% and 10% points in the temperature profiles, for both the integral and geometric methods, are plotted in Figure 6. It can be seen that, regardless of the choice of edge reference points, the inference is that the entrainment into the layer is strongly reduced as a function of heat release, amounting to about 50%, for a mean density in the layer of 40% below its nominal cold value. That the entrainment reduction is in excess of the mean density reduction suggests that the decrease in entrainment flux more than compensates for the additional displacement due to density change.

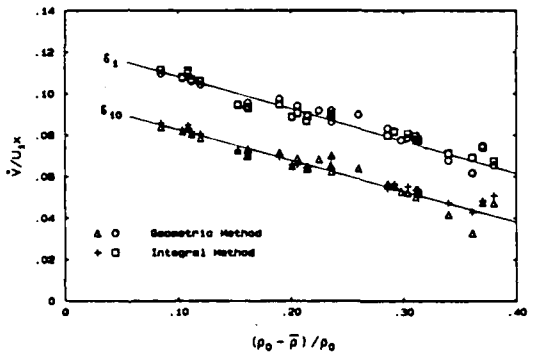


Fig. 6 Effect of Heat Release on Overall Layer Entrainment

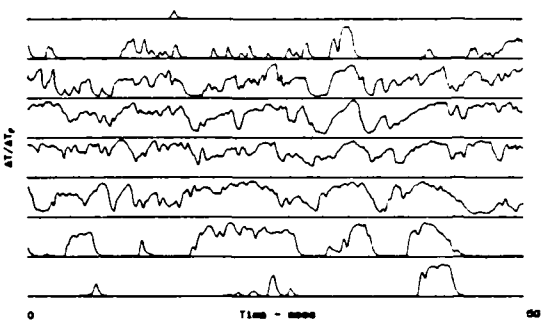


7a) 2% $F_2$ 2% $H_2$ $\Delta T_p$ = 186 K $\Delta T_{max}$ = 171 K

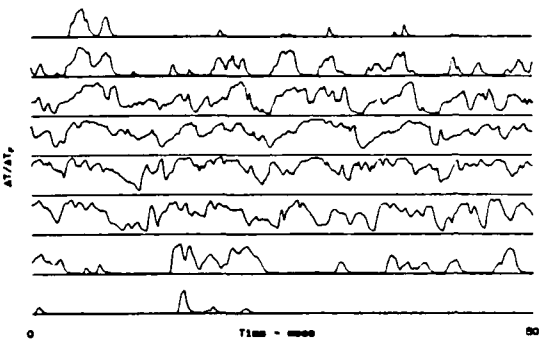


7b) 6% $F_2$ 6% $H_2$ $\Delta T_p$ = 553 K $\Delta T_{max}$ = 498 K

Fig. 7 Temperature vs. Time Traces

## II. Large Scale Structure Dynamics

Figures 7a and 7b show time traces of temperature from the rake of cold wires. Both runs are at $\phi$ = 1. The data in Figure 7a are from a run with 2% $F_2$ and 2% $H_2$, for a flame temperature rise of 186 K, Figure 7b shows the results of a run with 6% $F_2$ and 6% $H_2$, with a flame temperature rise of 553 K. At elevated temperatures, the flow dynamics still appear to be dominated by large scale structures separated by cold tongues of fluid which extend well into the layer. These findings are consistent with the earlier results at low temperatures[19,20,21].

Spark schlieren photographs are presented in Figures 8a and 8b, representing conditions of both low and high heat release. Figure 8a is a 2% $F_2$ and 2% $H_2$ run with an adiabatic flame temperature rise of 186 K. I Figure 8b is shown a 6% $F_2$ and 24% $H_2$ run with an adiabatic flame temperature rise of 847 K. The large scale structure is evident in both photographs and does not appear to be greatly altered by the heat release. Furthermore, that the structures appear well defined in the schlieren photographs suggests that they retain their predominately two-dimensional nature. Ganji & Sawyer[13] and Pitz & Daily[22] continued to observe the large scale structures behind a rearward facing step at higher temperatures still, corresponding to adiabatic flame temperatures of up to about 1650 K absolute. Keller & Daily[16] also observed that well-ordered structures were present for all values of heat release in their investigations.

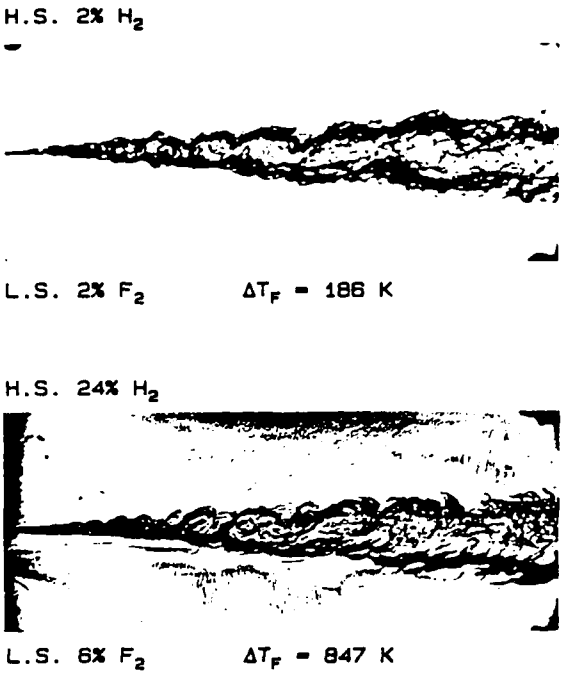


Fig. 8 Spark Schlieren Photographs of Reacting Shear Layers

## III. Pressure Gradient Results

It could be argued that, in combusting flows with substantial density variations and appreciable pressure gradients, an additional mixing mechanism might be operative, resulting from a possible relative acceleration between light fluid elements and heavy fluid elements[5,25]. The efficacy of such a mechanism would of course depend on the scales at which the density variations would be observed and their relation to the viscous small scales of the flow. If the hot/cold fluid elements are very closely spaced, viscous effects might not permit large relative motions to be established and little or no augmentation of the mixing would be observed. These issues were investigated, in part, in the experiments discussed below.

Setting the sidewalls for zero pressure gradient for the cold flow yields a naturally induced favorable pressure gradient in the case of flow with heat release. In this investigation, such favorable pressure gradient runs were made at reactant concentrations up to 6% $H_2$ and 6% $F_2$, corresponding to a flame temperature rise of 553K. This was sufficient to induce a pressure increment $\Delta p$, over the distance from the splitter plate tip to the measuring station, of about 1/2 of $\frac{1}{2}\rho_0 U_2^2$, the low speed free stream dynamic head. This caused the high speed velocity to increase from 21.2 to 22.3 m/s and the low speed velocity from 8.2 to 10.3 m/s between the splitter tip and the measuring station.

The resulting mean temperature profiles, with and without pressure gradient, are presented in Figure 9. The layer is thinned by the pressure gradient, as would be expected in accelerating flow. It can be seen, however, at least for the values of heat release and pressure gradient reported here, that there appears to be no significant change in either the peak temperature or the total amount of product formation induced by the favorable pressure gradient. Temperature profiles at lower temperatures also show no systematic changes resulting from pressure gradient, at least to within the estimated reproducibility and accuracy of the data (3 - 5%).

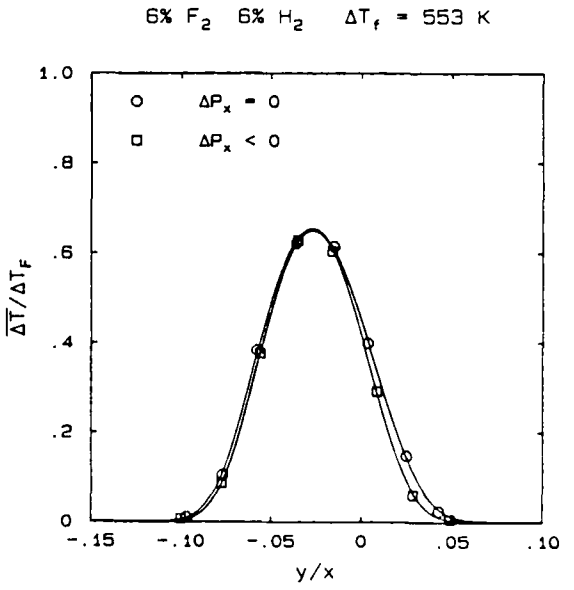


Fig. 9 Effect of Pressure Gradient on Mean Temperature Profile

## CONCLUSIONS

We have found that the growth rate of a chemically reacting shear layer with heat release does not increase and in fact appears to decrease slightly. In the presence of an increase in the shear layer displacement thickness as a result of heat release, one might have expected a commensurate increase in shear layer thickness. The implication is that the decrease in the entrainment flux must more than compensate for the displacement effect.

The imposition of a favorable pressure gradient is not found to have any noticeable effect on the amount of mixing and chemical production in the layer.

## ACKNOWLEDGEMENTS

The assistance of C. E. Frieler as well as the expert help of Mr. Earl E. Dahl in running the experiments reported here is greatly appreciated. We would also like to acknowledge many helpful discussions with Dr. J. E. Broadwell. This work was sponsored by the Air Force Office of Scientific Research (AFOSR) Contract No. F49620-79-C-0159 and Grant No. 83-0213.

## REFERENCES

[1] BATT, R. G. 1975 Some Measurements on the Effect of Tripping the Two-Dimensional Shear Layer. AIAA J. 13, 245-247

[2] BAULCH, D. L., DUXBURY, J., GRANT, S. J., and MONTAGUE, D. C. 1981 Evaluated Kinetic Data for High Temperature Reactions, Volume 4. J. Phys. Chem. Ref. Data, Vol. 10, Suppl. 1

[3] BERNAL, L. P., BREIDENTHAL, R. E., BROWN, G. L., KONRAD, J. H., and ROSHKO, A. 1979 On the Development of Three-Dimensional Small Scales in Turbulent Mixing Layers. In Turbulent Shear Flows 2, Second International Symp. on Turbulent Shear Flows, July 1979, Springer Verlag, 305-313

[4] BRADSHAW, P. 1966 The Effect of Initial Conditions on the Development of a Free Shear Layer. J. Fluid Mech., 26(2), 225-236

[5] BRAY, K. N. C. and LIBBY, P. A. 1981 Countergradient Diffusion in Pre-mixed Turbulent Flames. AIAA J. 19, 205-213

[6] BREIDENTHAL, R. E. 1978 A Chemically Reacting, Turbulent Shear Layer Ph.D. Thesis, Caltech; and 1981 Structure in Turbulent Mixing Layers and Wakes using a Chemical Reaction. J. Fluid Mech.,109, 1-24

[7] BROWAND, F. K. and LATIGO, B. O. 1979 Growth of the Two-Dimensional Mixing Layer from a Turbulent and Non-Turbulent Boundary Layer. Phys. Fluids, 22(6), 1011-1019

[8] BROWN, G. L. and ROSHKO, A. 1974 On Density Effects and Large Structure in Turbulent Mixing Layers. J. Fluid Mech. 64(4)), 775-816.

[9] BROWN, J. L. 1978 Heterogeneous Turbulent Mixing Layer Investigations Utilizing a 2-D 2-Color Laser Doppler Anemometer and using a Concentration Probe. Ph. D. Thesis, U. Missouri - Columbia

[10] CALDWELL, F. R. 1962 Thermocouple Materials. National Bureau of Standards Monograph 40, United States Department of Commerce, National Bureau of Standards

[11] COHEN, N. & BOTT, J. F. 1982 Review of Rate Data for Reactions of Interest in HF and DF Lasers. The Aerospace Corporation, Report SD-TR-82-86.

[12] DIMOTAKIS, P. E. 1984 Entrainment into a Fully Developed, Two - Dimensional Shear Layer. AIAA Paper 84-0368, Reno, Nevada

[13] GANJI, A. T. and SAWYER, R. F. 1980 Turbulence, Combustion, Pollutant, and Stability Characterization of a Premixed, Step Combustor. NASA CR 3230; and 1980 Experimental Study of the Flowfield of a Two-Dimensional Premixed Turbulent Flame, AIAA J., 18(7), 817-824

[14] HO, C. M. and HUERRE, P. 1984 Perturbed Free Shear Layers. Ann. Review Fluid Mech., Vol.16, 365-424

[15] KEE, R. J., MILLER, J. A., JEFFERSON, T. H. 1980 CHEMKIN: A General Purpose, Problem Independent, Transportable, Fortran Chemical Kinetics Code Package. SANDIA Report SAND80-8003

[16] KELLER, J. O. DAILY, J. W. 1983 The Effect of Large Heat Release on a Two Dimensional Mixing Layer. AIAA Paper 83-0472, Reno, Nevada

[17] KONRAD, J. H. 1976 An Experimental Investigation of Mixing in Two-Dimensional Turbulent Shear Flows with Application to Diffusion-Limited Chemical Reactions. Ph.D. Thesis, Caltech, and Project Squid Technical Report CIT-8-PU.

[18] KOOCHESFAHANI, M. M. 1984 Experiments on Turbulent Mixing and Chemical Reactions in a Liquid Mixing Layer. Ph. D. Thesis, California Institute of Technology

[19] MUNGAL,M. G., DIMOTAKIS,P. E. BROADWELL,J. E. 1984 Turbulent Mixing and Combustion in a Reacting Shear Layer AIAA Journal 22(6), 797-800

[20] MUNGAL, M. G. DIMOTAKIS, P. E. 1984 Mixing and Combustion with Low Heat Release in a Turbulent Shear Layer. J. Fluid Mech. 148 349-382

[21] MUNGAL,M. G., DIMOTAKIS,P. E. HERMANSON,J. C. 1984 Reynolds Number Effects on Mixing and Combustion in a Reacting Shear Layer. AIAA Paper 84-0371, Reno, Nevada

[22] PITZ, R. W. DAILY, J. W. 1983 Combustion in a Turbulent Mixing Layer Formed at a Rearward-Facing Step. AIAA Journal 21(11), 1565-1570

[23] REBOLLO, M. R. 1973 Analytical and Experimental Investigation of a Turbulent Mixing Layer of Different Gases in a Pressure Gradient. Ph.D. Thesis, Caltech

[24] SCADRON, M. D. WARSHAWSKY, I. 1952 Experimental Determination of Time Constants and Nusselt Numbers for Bare-Wire Thermocouples in High-Velocity Air Streams and Analytic Approximation of Conduction and Radiation Errors. NACA Technical Note 2599.

[25] SPALDING, D. B. 1984 The Two-Fluid Model of Turbulence Applied to Combustion Phenomena. AIAA Paper 84-0476, Reno, Nevada

[26] WALLACE, A. K. 1981 Experimental Investigation of the Effects of Chemical Heat Relese in the Reacting Turbulent Plane Shear Layer, Ph.D. Thesis, The University of Adelaide; also AFOSR Report AFOSR-TR-84-0650.

AIAA'85

AIAA-85-0056

# Measurements of Entrainment and Mixing in Turbulent Jets

W. J. A. Dahm and P. E. Dimotakis

California Institute of Technology
Pasadena, CA

**AIAA 23rd Aerospace Sciences Meeting**

January 14-17, 1985/Reno, Nevada

# MEASUREMENTS OF ENTRAINMENT AND MIXNG IN TURBULENT JETS

W.J.A. Dahm[1] and P.E. Dimotakis[2]

Graduate Aeronautical Laboratories
of the
California Institute of Technology
Pasadena, California 91125

## Abstract

An experimental investigation of entrainment and mixing in the self-similar far field of an axisymmetric free turbulent jet in water is presented. Length and time scales for the flame length fluctuations of reacting jets are shown to be approximately equal to the local characteristic large scale length and time of the flow. It is also shown that instantaneous radial profiles of concentration across the jet do not resemble the mean concentration profile, indicating that the mean profile is a poor representation of the mixed fluid states within the jet. These instantaneous profiles also show that unmixed ambient fluid is transported throughout the entire extent of the jet, and that the mixed fluid composition within the jet can be fairly uniform in regions extending across a large part of the local jet diameter. Lastly, the amount of unmixed ambient fluid on the jet centerline is found to vary roughly periodically with a period approximately equal to the local characteristic large scale time of the flow. These results suggest that large scale transport mechanisms, displaying a characteristic organization, play an important role in entrainment and mixing in the far field of turbulent jets.

## Introduction

Experimental investigations over the past decade have demonstrated that entrainment and mixing in fully turbulent shear layers is characterized by organization that results from the dynamics of large scale vortical motions. These large scale motions have been shown to transport unmixed fluid, from both free streams, across the entire extent of the layer ( Konrad[1] 1976, Breidenthal[2] 1978 ). Furthermore, as a consequence of these motions, the probability of finding mixed fluid within a given range of compositions is essentially uniform across the entire layer ( Konrad[1] 1976, Fiedler[3] 1974, Koochesfahani[4] 1984, Koochesfahani & Dimotakis[5] 1984). On the basis of these results and many others, it is now generally recognized that models of entrainment and mixing in turbulent shear layers probably need to incorporate features of these large scale motions.

Such large scale organized mixing may also be present in other free turbulent shear flows, including the axisymmetric free jet. The existence of organized vortical structure in the near field of turbulent jets has been recognized for some time (e.g. Bradshaw et al[6] 1964, Crow & Champagne[7] 1971). The prevailing view, however, is that this near field structure does not survive in any organized form beyond the first few jet diameters. Mixing in the far field of the jet is classically viewed as a stochastic process, involving transport by small scale eddies driven by gradients in the mean profiles, characteristically lacking any persistent large scale organization. This picture has arisen largely from point measurements and flow visualization techniques which are unable to reveal the internal structure of the mixing.

However, the results of several recent investigations ( Tso et al[8] 1981, Dimotakis et al[9] 1983a, Dimotakis et al[10] 1983b, Dahm et al[11] 1984 ) have suggested that the relevant transport mechanisms in the far field of turbulent jets may be quite different from this classical picture and may exhibit a large scale organization similar in many respects to that found in shear layers. To investigate this prospect further, the measurements presented here were conducted to study several aspects of entrainment and mixing in turbulent jets.

---

[1] Presently, Graduate Student, Aeronautics

[2] Assoc. Professor, Aeronautics & Applied Physics



AIAA Paper 85-0056

## Experimental Methods

Three sets of measurements of entrainment and mixing in the self-similar far field of an axisymmetric momentum-driven free turbulent jet in water ( $Sc \approx 600$ ) are described below. These measurements were all carried out in a water facility, documented previously[9,11], using laser induced fluorescence (LIF) techniques.

### I. Flame length fluctuations of reacting jets

The chemically-sensitive LIF technique[9,10,11] was used in conjunction with an (isothermal) acid-base reaction to determine length and time scales for the flame length fluctuations of chemically reacting jets.

Briefly, an alkaline jet premixed with a small amount of a pH-sensitive laser-fluorescent dye was discharged through an axisymmetric nozzle into a large acidic reservoir. By appropriately selecting the initial absolute concentrations of the acid and base solutions, the pH-sensitive characteristics of the dye could be exploited so that mixed fluid illuminated by the laser excitation would fluoresce only if the local mass ratio of ambient fluid to jet fluid mixed at the molecular scale did not exceed a threshold value, referred to here as the reaction stoichiometric ratio $\phi$. This ratio could be selected by choosing the relative initial concentrations of the acid and base solutions. The fluorescence transition was reversible and occured over a very narrow range of the mixture ratio. By arranging the laser light to form either a single thin sheet containing the jet axis or a pair of mutually orthogonal sheets both containing the jet axis, the jet fluid in the plane of the laser sheet(s) that had not yet mixed, on a molecular scale, with ambient fluid in excess of the selected stoichiometric ratio could be visualized directly.

Earlier measurements (Dahm et al[11] 1984) using this technique have demonstrated a nearly periodic fluctuation of the "flame" length of such reacting jets. A composite sequence showing these fluctuations, consisting of every fifth frame from an excerpt of a high speed motion film of such a chemically reacting turbulent jet visualized using this technique, is shown in figure 1. In each frame, the fluorescence from each of a pair of mutually orthogonal laser sheets, both containing the jet axis, was imaged by a system of mirrors without perspective distortion onto the film plane to allow a simultaneous view of mixing in the two thin, orthogonal slices through the jet.

While the effects of heat release and density changes that accompany combustion are not addressed in experiments with such simple acid-base reactions in water, experience in turbulent mixing layers has shown that the basic ideas suggested by such investigations remain applicable when combustion is present. Indeed, when properly normalized, the mean flame lengths of momentum-driven turbulent jets in water[11,12] and in highly exothermic gas flames[13-17] as well as in liquid-vapor condensation systems[18-20] are in good agreement, as shown in figure 2. Such a correlation was demonstrated by Avery & Faeth[18] (1974). Broadwell[21] (1982) uses a similar form, for water and gas flames, to argue that the rate of molecular mixing is set by the rate of entrainment for the jet. Figure 2 then demonstrates that, at Reynolds numbers sufficiently large for mixing to become entrainment-limited, the flame length of any reacting jet is determined solely from the generic scaling laws for jet entrainment expressed in momentum variables.

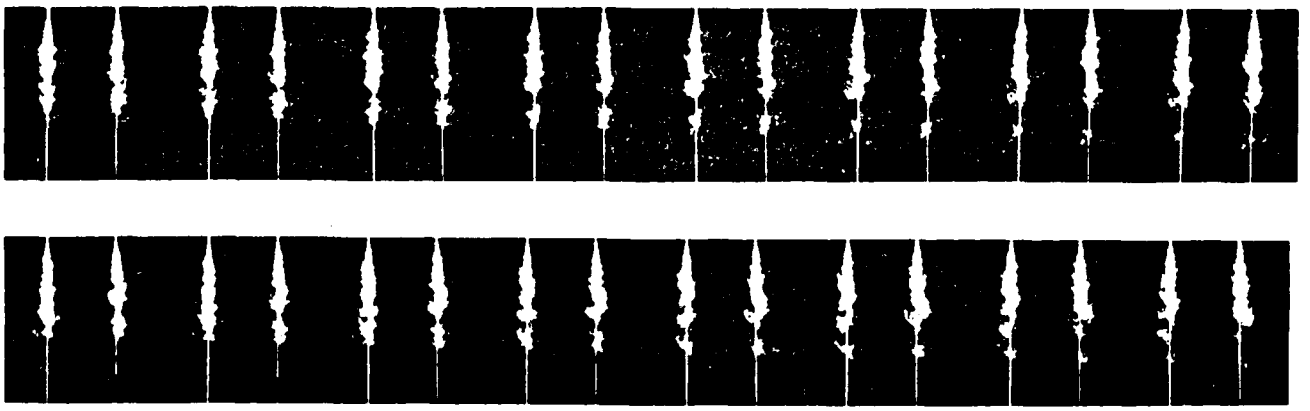

Figure 1. Composite time sequence from a motion film of a chemically reacting turbulent jet, visualized using the dual-orthogonal planar LIF technique, showing the flame length fluctuations; $\phi = 15$, $Re = 10{,}000$.

The correlation in figure 2 arises from the normalization with d*, the jet "momentum diameter", defined as

$$d^* = \frac{2\,\dot{m}_o}{(\pi \rho_\infty J_o)^{1/2}}$$

where $\dot{m}_o$ is the jet exit mass flux, $J_o$ is the jet momentum flux, and $\rho_\infty$ is the ambient fluid density. This momentum diameter was introduced in a limited context by Thring & Newby[22] (1952), and has been used by Becker et al[15,16] (1978) in gas flames. However, figure 2 suggests a general scaling with d* for all momentum jets, and indicates a proper dimensionless form for the axial coordinate x of the far field of all momentum-driven turbulent jets as

$$\chi = x/d^*$$

In the present experiment, the instantaneous turbulent flame length was measured directly, using a coordinate digitizer, from each of over 2400 individually projected film frames of a high speed motion film of such a reacting jet at Re = 10,000 and $\phi = 15$. The resulting data spanned roughly 50 periods of the flame fluctuation. Length and time scales for these fluctuations were determined from the measurements and compared with the local characteristic large scale length and time of the flow, respectively the local jet visual diameter $D = 0.4x$ at the mean flame tip location x, and $D/U_c$ where $U_c = 6\,(J_o/\dot{m}_o)\,x^{-1}$ is the mean centerline velocity at the flame tip.

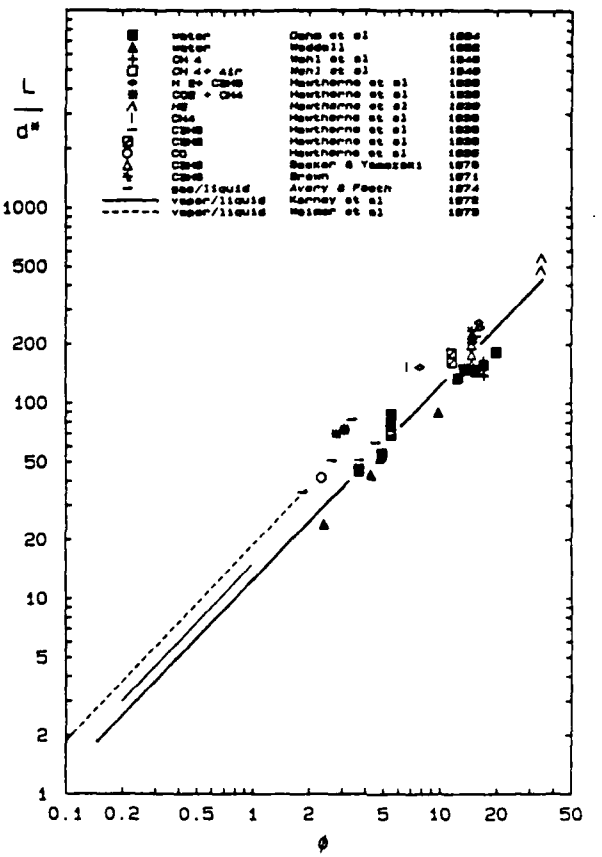


Figure 2. Dimensionless mean length, L, of momentum-driven turbulent jet flames as a function of their reaction stoichiometric ratio, $\phi$, for isothermal reactions in water, exothermic gas reactions and liquid-vapor condensation reactions. (Buoyancy effects are present to various degrees in some of these data.)

## II. Radial profiles of concentration in non-reacting jets

Instantaneous radial profiles of jet fluid concentration in a non-reacting jet were measured with high resolution using a passive LIF imaging technique in conjunction with high speed digital data acquisition and digital image display methods. The technique was similar to earlier measurements of concentration in the plane shear layer (Koochesfahani & Dimotakis[5] 1984).

The laser fluorescent dye was again premixed with the jet fluid (water), and discharged into the ambient reservoir fluid (water). In this case, no chemical reaction was involved. The beam (514.5 nm) from an argon ion laser was collimated and oriented to cross the jet radially, perpendicular to the jet axis. The fluorescence from dye along the beam was imaged onto a 1024-element Reticon self-scanning linear photodiode array, the sequential pixel output of which gave consecutive instantaneous profiles of the fluorescence intensity. A green filter effectively eliminated directly scattered laser light from any particulates in the flow.

Radial profiles of fluorescence intensity were measured at $\chi = 300$ for Re = 1500 and Re = 5000, on either side of the Re = 3000 asymptotic threshold (Dahm et al[11] 1984) at which mixing in the far field of such jets in water becomes entrainment-limited and, therefore, the flame length becomes independent of Reynolds number.

The photodiode array was clocked at a pixel rate of 256 kHz, corresponding to a scan rate of 235 scans/sec and a scan time of 4.3 msec, which was several orders of magnitude faster than any relevant local time scales in the flow at either Reynolds number. Consequently, temporal resolution was not an issue in these measurements.

Each of the 1024 photodiode array elements (pixels) had a sensitive detector aperture of

25μm × 26μm. The optics used produced an image ratio of 26:1, and the beam diameter varied from roughly 0.5mm to about 1mm, thereby defining the measurement volume for each pixel. The resulting resolution was sufficient to resolve even the smallest turbulent scales of motion at the lower Reynolds number. At neither Reynolds number could the strain-limited diffusion layer thickness ( Batchelor scale ) be resolved, which is of the order $Sc^{-1/2}$ smaller than the Kolmogorov scale.

The array output was digitized through a single channel high-speed 8-bit A/D converter and recorded on a computer disk. Since the scan time was fast relative to the local time scales in the flow, and in order to keep the amount of data collected manageable, only every 16th scan of the array was actually recorded on the disk at Re = 1500, and every 6th scan at Re = 5000. Each measurement consisted of 4000 recorded scans of the array (in excess of 4 million measurements) spanning approximately 12 local characteristic large scale flow times, this limit being imposed by the local flow duration.

The measured pattern of dark noise and background illumination was subtracted from these data. The resulting measured fluorescence intensity profiles could then be converted to profiles of jet fluid concentration as described below ( see also Koochesfahani & Dimotakis[5] 1984).

The intensity of fluorescence measured by the photodiode array, $F(\xi,t)$, was locally related to the instantaneous dye concentration and beam intensity at every point along the beam as

$$F(\xi,t) = h(\xi) \cdot J[c(\xi,t)]\, I(\xi,t)$$

where $\xi$ is a coordinate along the beam in the direction of propagation and $c(\xi,t)$ is the instantaneous dye concentration profile along the beam. Here, $I(\xi,t)$ is the instantaneous beam intensity profile, $J[c]$ relates the local intensity of fluorescence to the local beam intensity, and $h(\xi)$ is the transfer function relating the fluorescence intensity to that measured by the photodiode array.

The instantaneous beam intensity profile $I(\xi,t)$ was, in turn, related to the dye concentration profile $c(\xi,t)$ through the attenuation integral

$$I(\xi,t) = I_o(t)\, \frac{A_o}{A(\xi)}\, \exp\left( -\int_0^{\xi} J[c(\lambda,t)]\, d\lambda \right)$$

where $I_o(t)$ is the beam intensity at $\xi = 0$ and $A(\xi)$ is the beam cross sectional area profile. Over the range of concentrations in this experiment, $J[c]$ was determined by a calibration to be linearly related to the dye concentration as

$$J[c] = \zeta \cdot c$$

where the constant $\zeta$, related to the scattering cross section of the dye, was determined from the calibration.

Defining an overall transfer function $H(\xi)$ to include the beam area variation, namely

$$H(\xi) = h(\xi)\, \frac{A_o}{A(\xi)} ,$$

gave the instantaneous fluorescence intensity profile measured by the photodiode array as

$$F(\xi,t) = I_o(t)\, H(\xi)\, \zeta\, c(\xi,t)\, \exp\left( -\zeta \int_0^{\xi} c(\lambda,t)\, d\lambda \right) .$$

The transfer function $H(\xi)$ was determined from an in situ measurement of $F(\xi)$ at a uniform dye concentration $c_1$ as

$$\left[ H(\xi) / H(\xi^*) \right] = \left[ F(\xi) / F(\xi^*) \right] \exp\left( \zeta\, c_1\, (\xi - \xi^*) \right)$$

where $\xi^*$ was an arbitrary reference location. $H(\xi)$ represents, therefore, an accounting of the collective non-idealities in the optical system and the array.

Normalizing each instantaneous measured fluorescence intensity profile by its value at $\xi^*$, where the dye concentration was at a constant reference value $c^*$, gave the dye concentration profile relative to this reference as

$$\frac{c(\xi,t)}{c^*} = \frac{\left[ F(\xi,t) / F(\xi^*,t) \right]}{\left[ H(\xi) / H(\xi^*) \right]}\, \exp\left( \zeta \int_{\xi^*}^{\xi} c(\lambda,t)\, d\lambda \right) .$$

A small vessel, positioned about one-and-a-half local jet diameters from the centerline, containing a circulating dye solution at a known concentration, was also imaged onto the array to set this reference condition.

Denoting the known concentration of dye issuing from the jet exit as $c_o$ defined the instantaneous jet fluid concentration profile $c_j(\xi,t)$ in terms of the dye concentration profile as

$$c_j(\xi,t) = \frac{c(\xi,t)}{c_o}$$

The jet fluid concentration profile along the beam corresponding to each measured fluorescence intensity profile could then be determined as

$$\frac{c_j(\xi,t)}{c_j^*} = \frac{[\,F(\xi,t)/F(\xi^*,t)\,]}{[\,H(\xi)/H(\xi^*)\,]} \exp\left(\zeta c_o \int_{\xi^*}^{\xi} c_j(\lambda,t)\,d\lambda\right)$$

The resulting instantaneous profiles of jet fluid concentration were expressed in the conventional radial self-similar form $g(n,t)$, where $n = r/x$, by normalizing each individual profile with the mean centerline concentration as

$$g(n,t) = \frac{c_j(n,t)}{\overline{c}_j(0)} .$$

III. Unmixed ambient fluid on the jet axis

The probability of unmixed ambient fluid appearing at a point on the jet axis was measured as a function of time for Re = 1500 and Re = 5000 using a passive LIF technique.

The laser beam was oriented coincident with the jet centerline. The laser dye was again premixed with the jet fluid, and the fluorescence from a segment along the beam centered at $\chi = 300$ and extending from $285 < \chi < 315$ (roughly one-fifth the scale of the local jet diameter) was imaged onto the 1024-element Reticon linear photodiode array. A green filter was again used to block directly scattered laser light. As before, the array was scanned at 256 kHz and the output from every 16th scan at Re = 1500 and every 6th scan at Re = 5000 was recorded. The data for each of these measurements consisted of 4000 scans of the array, again spanning approximately 12 local characteristic large scale flow times.

In this case, however, it was not necessary to convert the measured fluorescence intensities to jet fluid concentration, as was done in the previous experiment, but only to distinguish between mixed and unmixed fluid. Consequently, a reference condition was not used in this measurement. The threshold between mixed and unmixed fluid was determined from the peak dark noise in the array. The fraction of the 1024 pixels imaging unmixed ambient fluid, corresponding to the probability of finding unmixed fluid, could subsequently be determined as a function of time.

## Results and Discussion

I. Flame length fluctuations of reacting jets

The instantaneous turbulent flame length as a function of time is shown in figure 3 for Re = 10,000 and $\phi = 15$. The nearly regular length fluctuations of figure 1 are evident in these data. Defining (albeit, somewhat subjectively) fluctuation events, delimited by tic marks in figure 3, allows a length and time scale to be determined for each fluctuation event.

Histograms of the resulting fluctuation length and time scales, normalized by the corresponding local characteristic large scale quantities, are shown in figure 4. The histograms indicate that the flame length fluctuations of reacting jets occur on a length and time scale approximately equal to the local characteristic large scales of the flow.

These fluctuations can be interpreted in the context of the instantaneous concentration field of the jet. Their length and time scaling show that the mixed fluid composition in a large region of the jet crosses the reaction stoichiometric ratio within one local characteristic large scale time, suggesting that this fluid is within a fairly narrow range of compositions. Such regions of qualitatively uniform jet fluid concentration have been inferred from still photographs of planar fluorescence in jets (Dimotakis et al[10] 1983b). The flame length fluctuations are, therefore, directly indicative of a nearly periodic large scale organization of mixing in the jet far field.

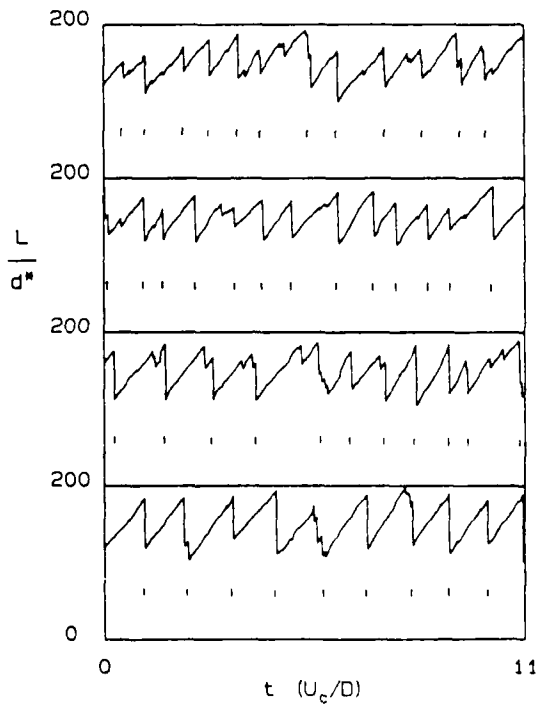


Figure 3. Instantaneous turbulent flame length vs. time; $\phi = 15$, Re = 10,000.

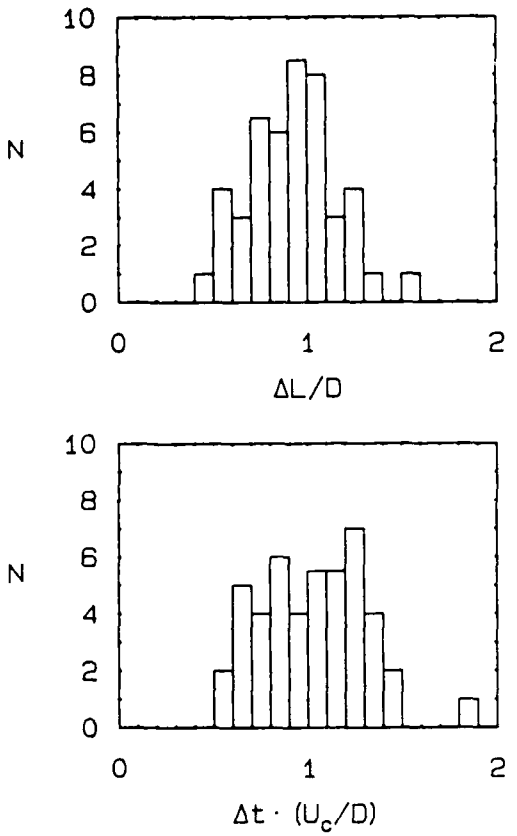


Figure 4. Histograms of length and time scales for the flame length fluctuations in figure 3, normalized by the corresponding local characteristic large scale flow quantities.

Hussain[23] (1983) has suggested that the significance of organization in turbulent shear flows has been overemphasized. The flame length fluctuations, however, suggest that this large scale organization plays a crucial role in the entrainment, mixing and chemical reaction processes in the jet. It is noteworthy that similar flame length fluctuations have also been reported in combustion studies in buoyant plume flows (Zukoski et al[24] 1984).

## II. Radial profiles of concentration in non-reacting jets

The mean radial concentration profile at Re = 5000, determined by an ensemble average of the individual instantaneous profiles measured in these experiments, is compared in figure 5a in the radial similarity variable $\eta = r/x$ with the profiles reported in other experiments[25-31]. Note that this form of the radial variable $\eta$ does not force the profiles to match at the jet half-width, and thus provides a more rigorous comparison than does normalization of the radial coordinate by the

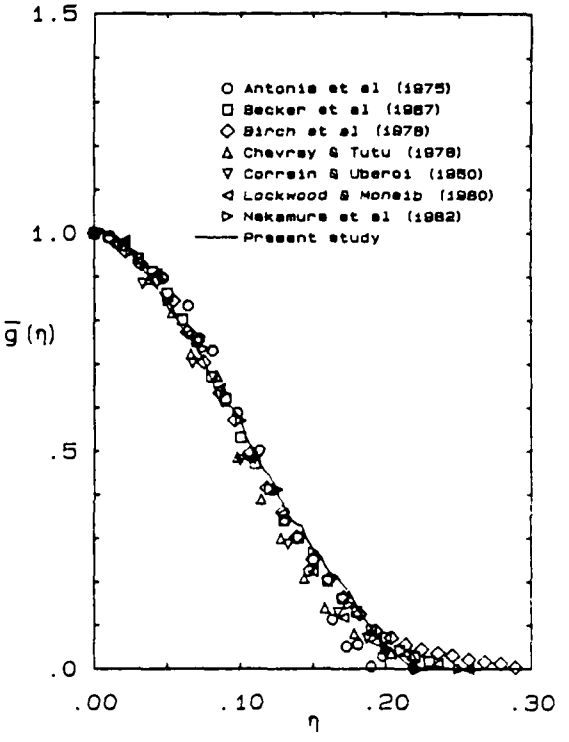


Figure 5a. Mean radial profile of jet fluid concentration (in self-similar form) compared with other experiments.

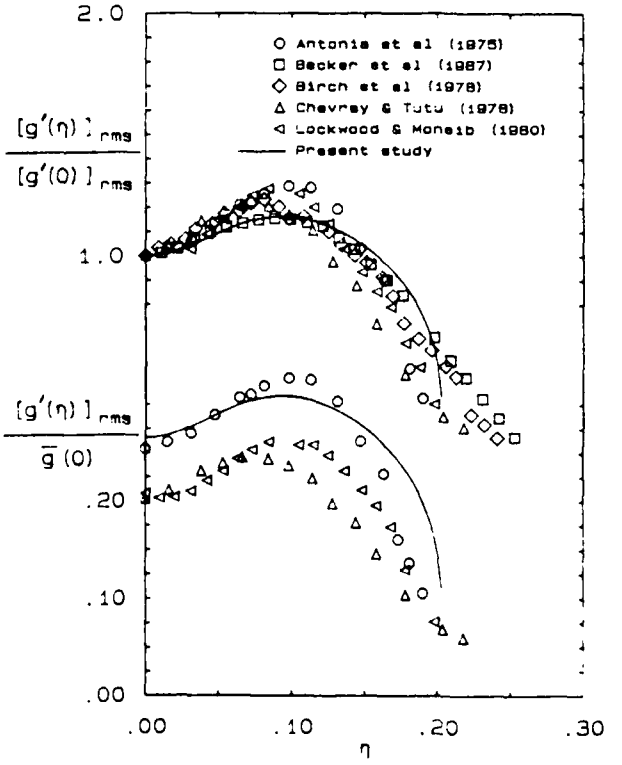


Figure 5b. Radial profile of rms concentration fluctuations (in self-similar form) compared with other experiments.

concentration half-width. Similarly, the radial profile of rms concentration fluctuations is shown in figure 5b. However, the principal emphasis in the present experiments is on high resolution measurements at a large number of points across the jet and, consequently, the duration over which these measurements extend is relatively short. Nevertheless, despite the limited statistical significance of mean profiles obtained from these data, the comparisons in figures 5a and 5b are quite good and serve to validate the measurements.

Several representative instantaneous radial concentration profiles at Re = 5000, each covering the entire radial extent of the jet, are shown in figures 6a-d.

Perhaps the most significant feature of the instantaneous profiles is how little they resemble the mean profile. Most of the instantaneous profiles are either of a "top-hat" type, such as figures 6c and 6d, where the mixed fluid across the entire jet diameter is within a fairly narrow range of concentrations (relative to what the mean profile suggests), or of a "two-level" type, such as figures 6a and 6b, where the mixed fluid in a large region near the jet axis is within one such narrow range of concentrations, while the mixed fluid across the remainder of the jet is within a second, lower range of concentrations. Broadwell & Breidenthal[32] (1982) have noted that such qualitative uniformity in the mixed fluid composition can, in retrospect, also be recognized in concentration profiles from plane turbulent jets by Uberoi & Singh[33] (1975), but that these authors do not remark about the shape of their profiles.

Furthermore, the profiles in figure 6 show that unmixed ambient fluid can be found throughout the jet. This has been observed in still photographs of planar fluorescence in jets (Dimotakis et al[9] 1983a), and supports the proposal that the classical notion of entrainment and mixing by stochastic small scale eddies may not be a good picture of the relevant transport mechanisms in the jet far field.

The mean concentration profile of figure 5a then results from an average of the mixed fluid profiles described above and the unmixed fluid within the jet, but is itself a poor representation of the compositions within the jet. This contrasts with the classical picture of turbulent mixing, in which instantaneous concentration profiles are presumed to qualitatively resemble the mean profile with small turbulent fluctuations about the mean, and may have particularly important implications for the modeling and prediction of chemical reactions between the mixed and unmixed fluids.

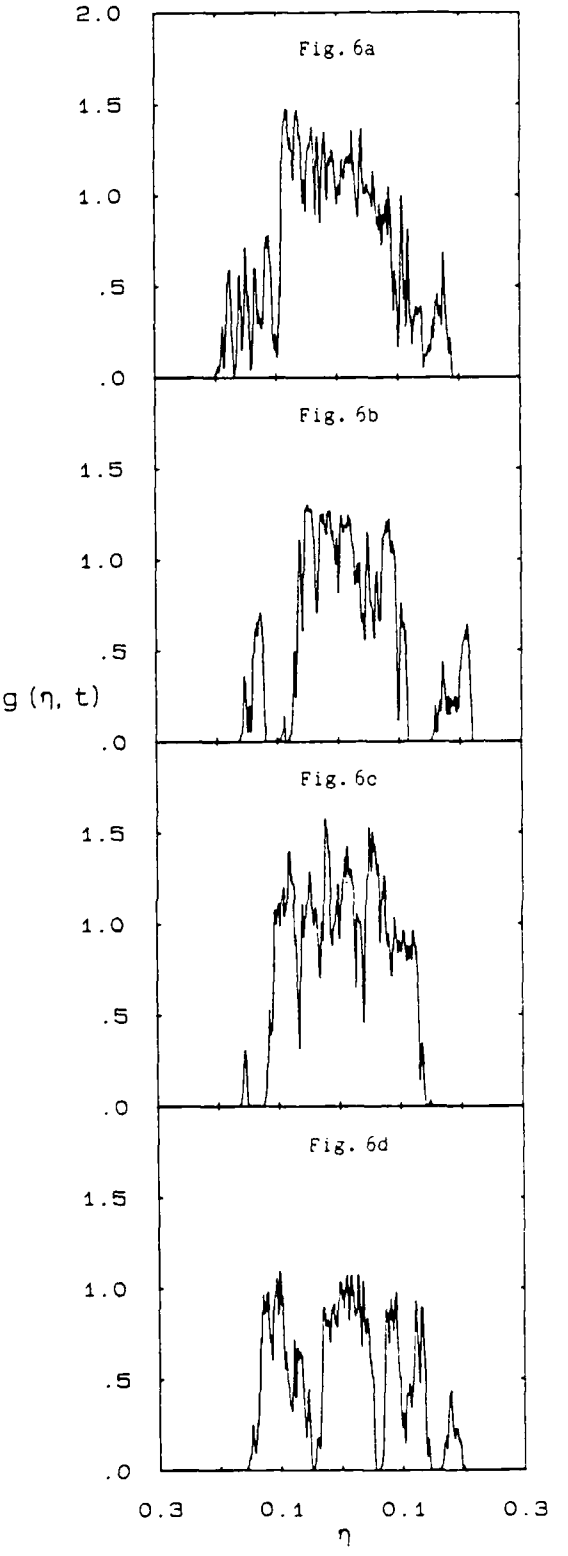


Figure 6. Representative instantaneous radial profiles of concentration across the jet; $x = 300$, Re = 5000.

The instantaneous concentration profile shapes in figures 6a-d as well as the observed flame length fluctuations of figures 2 and 3 can be interpreted in terms of the simple conceptual picture of mixing in the jet far field shown in figure 7, described by Dimotakis et al[10] (1983b). In this picture, large regions within the jet contain mixed fluid in a fairly narrow range of compositions, intertwined with unmixed ambient fluid. As a result, concentration profiles across the jet will have either the "top-hat" or "two-level" shape noted above, while the mixed fluid concentration along the axial direction decreases in a roughly step-wise fashion, following the requisite $x^{-1}$ form in the mean, and giving rise to the flame length fluctuations in a reacting jet.

A method for simultaneously interpreting many of these measured instantaneous concentration profiles is shown in figure 8. These pictures are similar to earlier displays of LIF data in a plane mixing layer (Koochesfahani & Dimotakis[5] 1984.) They are photographs of a digital image display screen, on which the digitized concentration data from the 512 array elements centered on the jet axis were displayed for 500 consecutive recorded array scans.

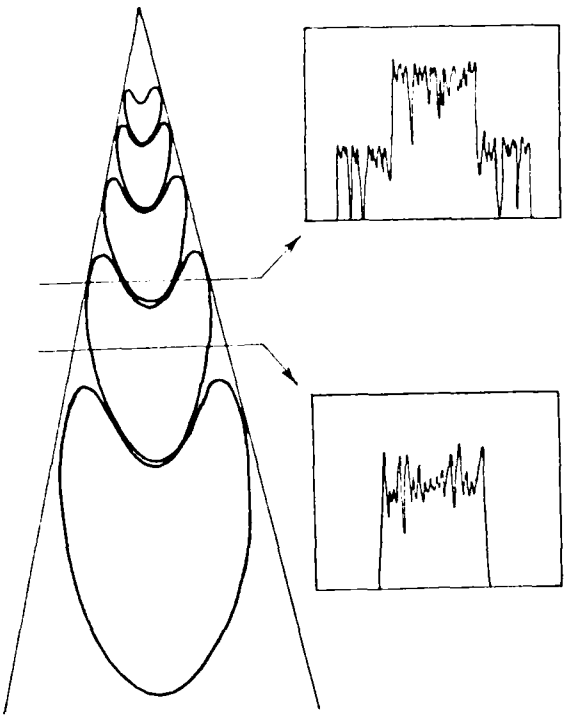

Figure 7. Idealized conceptual picture of the instantaneous concentration field of the turbulent jet.


Fig. 8a Re = 1500.


Fig. 8b Re = 5000.

Figure 8. r-t reconstruction of the turbulent jet concentration field from 500 sequential measured concentration profiles; $x = 300$.

The 256 different grey levels are assigned to denote the various concentration levels, with pure white representing $g(n,t) = 1.5$ and decreasing linearly to pure black denoting unmixed ambient fluid, namely $g(n,t) = 0$. These are, therefore, r-t pictures of the concentration along a line across the jet. It must be emphasized that these are not equivalent to still photographs of the concentration field in a plane intersecting the jet, as becomes evident near the jet edges.

It is apparent in the data in figure 8 that, at both Reynolds numbers, unmixed ambient fluid is transported throughout the entire radial extent of the jet. This figure also suggests that the topology of a stoichiometric surface between the mixed and unmixed fluids, commonly used in combustion studies, may be considerably more complex than that which might be suggested by a conventional small scale transport picture of jet mixing. Furthermore, as the individual concentration profiles in figure 6 suggested, the data in figure 8 show that the instantaneous mixed fluid composition can be fairly uniform, relative to what the mean concentration profile would suggest, across a large part of the local jet diameter.

A composite sequence from consecutive photographs of the type displayed in figure 8 is shown for each Reynolds number in figure 9. Each of these sequences displays roughly 2 million individual measurements. This method of displaying the measured profiles allows a direct interpretation of the time-varying concentration field in these data. The transport of unmixed ambient fluid throughout the jet, as well as regions of fairly uniform mixed fluid concentration extending across a large part of the local jet diameter, can again be discerned in these pictures. Note that a length increment along the jet centerline in the pseudo-axial (temporal) direction can be made roughly equivalent to a corresponding increment in the radial direction by a 50% stretching of the temporal direction.

## III. Unmixed ambient fluid on the jet axis

The fraction of the array detecting unmixed ambient fluid along the imaged segment of the jet axis is shown as a function of time for both Reynolds numbers in figure 10.

These data show that the probability of finding unmixed ambient fluid at a point on the jet axis shows a marked increase at roughly periodic intervals. Furthermore, as indicated by the time scale accompanying each trace, these increases are

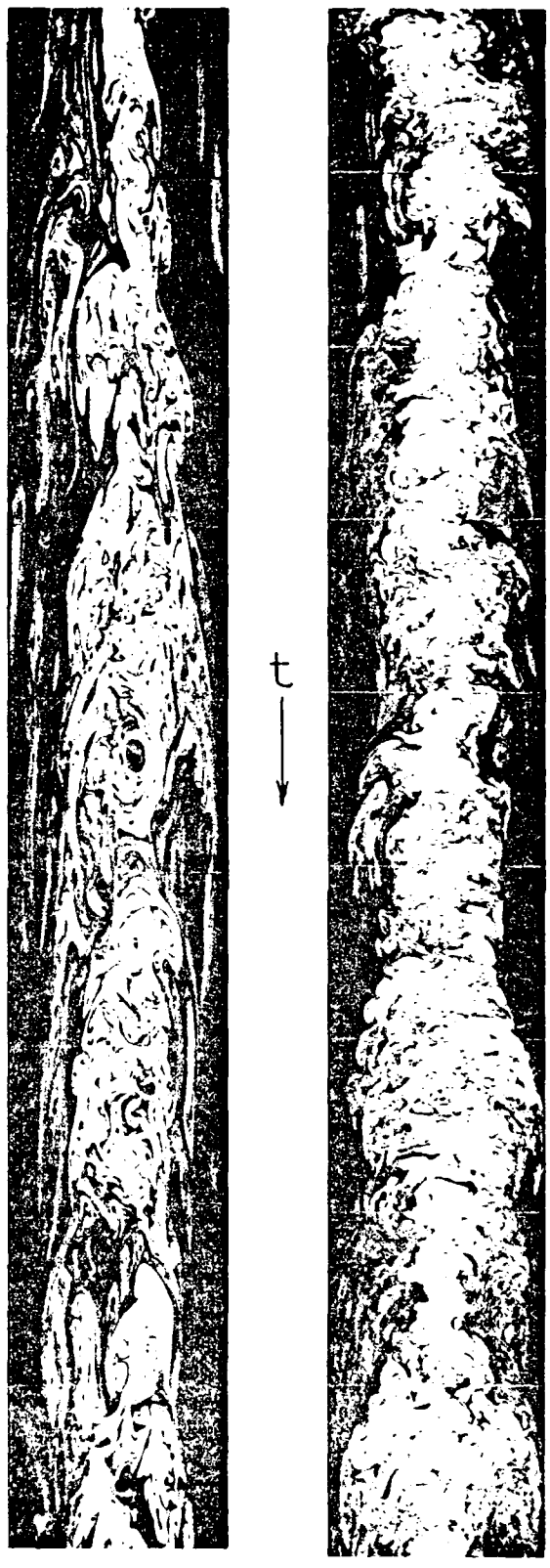


Fig. 9a Re = 1500. Fig. 9b Re = 5000.

Figure 9. Composite r-t reconstruction of the turbulent jet concentration field from 4000 sequential measured concentration profiles; $x = 300$.

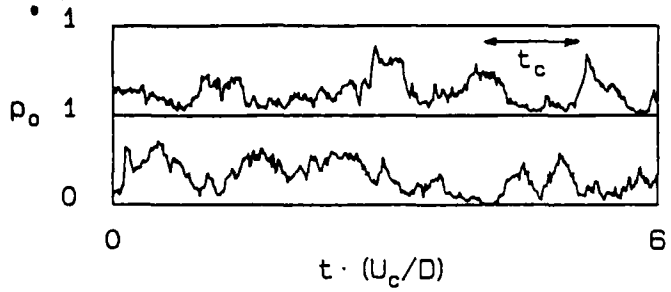


Fig. 10a Re = 1500.

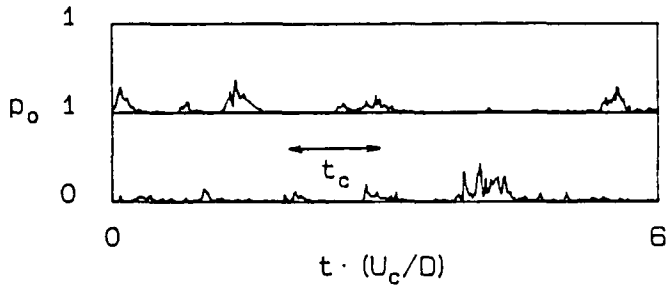


Fig. 10b Re = 5000.

Figure 10. Fraction of the imaged segment on the jet centerline detecting unmixed ambient fluid vs. time; $x = 300$.

typically separated by about one local characteristic large scale flow time. This roughly periodic increase in the probability of finding unmixed ambient fluid on the jet axis is consistent with the large scale entrainment mechanism proposed by Dimotakis et al[9] (1983a) and with the conceptual picture of jet mixing in figure 7.

In figure 10, the time-averaged probability of detecting unmixed ambient fluid at a point on the jet axis is 29% at Re = 1500, while at Re = 5000 this value is 3%. This difference may, to a certain extent, be ascribed to the decrease in relative resolution of the measurement at the higher Reynolds number. The effect of resolution on these measurements, however, may be determined by averaging the LIF intensity over two or more pixels before applying the mixed/unmixed criterion. The result of such a procedure indicates that, when the effective resolution at Re = 1500 is made equivalent to that in the original measurement at Re = 5000, the time averaged probability of detecting unmixed fluid is still 24%. While we might be led to conclude from this that less unmixed ambient fluid reaches the centerline at the higher Reynolds number, it is also possible that the spectrum of scales at which unmixed fluid is found, relative to the Kolomogorov scale, undergoes a shift toward higher wavenumbers as the Reynolds number is increased, and that consequently less unmixed fluid is detected. In other words, the flow at Re = 1500 may, in this respect at least, be qualitatively different than that at Re = 5000, an idea that is supported by the observation that reacting jets in water attain their asymptotic flame lengths at Re = 3000[11]. This question, however, must ultimately be resolved using other techniques.

## Conclusions

The results of these measurements, together with previous investigations[9,10,11], indicate that large scale transport mechanisms play an important role in entrainment and mixing in the far field of turbulent jets, and that the jet far field is characterized by large scale organization.

Instantaneous profiles of concentration across the jet show that, at any instant, the mixed fluid concentration can be fairly uniform within large regions in the jet, and that unmixed ambient fluid can be found throughout the jet. These characteristics of the instantaneous profiles as well as the measurements of unmixed fluid within the jet are consistent with a simple conceptual picture of large scale organization of entrainment and mixing in jets. For the case of chemically reacting jets, this organization manifests itself as a nearly periodic large scale fluctuation of the flame length, indicating the important role that such large scale organization plays in mixing in the far field of turbulent jets.

## Acknowledgements

The work reported here was sponsored, in part, by the Gas Research Institute (GRI) under Grant no. 5083-260-0878, and by the Energy and Environmental Research Corporation (EERC) under Contract no. 8400-28 on behalf of the Energy and Environmental Protection Agency (EPA), as well as by the Air Force Office of Scientific Research (AFOSR) under Contract no. F49620-79-0159 and Grant no. 83-0213.

## References

1. KONRAD, J.H. (1976), "An experimental investigation of mixing in two-dimensional turbulent shear flows with application to diffusion-limited chemical reactions", Ph.D. thesis, Caltech, Pasadena, California, also Project SQUID Technical Report CIT-8-PU.

2. BREIDENTHAL, R.E. (1978), "A chemically reacting turbulent mixing layer", Ph.D. thesis, Caltech, Pasadena, California.

3. FIEDLER, H.F. (1974), "Transport of heat across a plane turbulent mixing layer", Adv. Geophys., 18A, 93.

4. KOOCHESFAHANI, M.M. (1984), "Experiments on turbulent mixing and chemical reactions in a liquid mixing layer", Ph.D. thesis, Caltech, Pasadena, California.

5. KOOCHESFAHANI, M.M. and DIMOTAKIS, P.E. (1984), "Laser induced fluorescence measurements of concentration in a plane mixing layer", AIAA Paper no. 84-0198.

6. BRADSHAW, P., FERRISS, D.H. and JOHNSON, R.F. (1964), "Turbulence in the noise-producing region of a circular jet", J. Fluid Mech., 19, 591.

7. CROW, S.C. and CHAMPAGNE, F.H. (1971), "Orderly structure in jet turbulence" J. Fluid Mech., 48, 547.

8. TSO, J., KOVASNAY, L.S.G. and HUSSAIN, A.K.M.F. (1981) "Search for large scale coherent structures in the nearly self-preserving region of a turbulent axisymmetric jet", Transactions of the ASME, J. Fluids Engr., 103, 503.

9. DIMOTAKIS, P.E., MIAKE-LYE, R.C. and PAPANTONIOU, D.A. (1983a), "Structure and dynamics of round turbulent jets", Physics of Fluids, 26, 3185.

10. DIMOTAKIS, P.E., BROADWELL, J.E. and HOWARD, R.D. (1983b), "Chemically reacting turbulent jets", AIAA Paper no. 83-0474.

11. DAHM, W.J.A., DIMOTAKIS, P.E. and BROADWELL, J.E. (1984), "Non-premixed turbulent jet flames", AIAA Paper no. 84-0369.

12. WEDDELL, D.S. (1952), in Hottel, H.C., "Burning in laminar and turbulent fuel jets", Fourth (International) Symposium on Combustion, The Williams and Wilkins Co., 97.

13. WOHL, K., GAZLEY, C. and KAPP, N. (1948), "Diffusion flames", Third (International) Symposium on Combustion, The Williams and Wilkins Co., 288.

14. HAWTHORNE, W.R., WEDDELL, D.S. and HOTTEL, H.C. (1948), "Mixing and combustion in turbulent gas jets", Third (International) Symposium on Combustion, The Williams and Wilkins Co., 266.

15. BECKER, H.A. and YAMAZAKI, S. (1978), "Entrainment, momentum flux and temperature in vertical free turbulent diffusion flames", Comb. and Flame, 33, 123.

16. BECKER, H.A. and LIANG, D. (1978), "Visible length of vertical free turbulent diffusion flames", Comb. and Flame, 32, 115.

17. BROWN, A.P.G. (1971), "Structure of the round free turbulent propane-air diffusion flame", Ph.D. thesis, Queen's University, Kingston, Canada.

18. AVERY, J.F. and FAETH, G.M. (1974), "Combustion of a submerged gaseous oxidizer jet in liquid metal", Fifteenth (International) Symposium on Combustion, The Combustion Institute, 501.

19. KERNEY, P.J., FAETH, G.M. and OLSON, D.R. (1972), "Penetration characteristics of a submerged steam jet", AIChE J, 18, 548.

20. WEIMER, J.C., FAETH, G.M. and OLSON, D.R. (1973), "Penetration of vapor jets submerged in subcooled liquids", AIChE J, 19, 552.

21. BROADWELL, J.E. (1982), "A model of turbulent diffusion flames and nitric oxide production. Part I.", TRW Document No. 38515-6001-UT-00.

22. THRING, M.W. and NEWBY, M.P. (1952), "Combustion length of enclosed turbulent jet flames", Fourth (International) Symposium on Combustion, The Williams and Wilkins Co., 789.

23. HUSSAIN, A.K.M.F. (1983), "Coherent structures - reality and myth", Physics of Fluids, 26, 2816.

24. ZUKOSKI, E.E., CETEGEN, B. and KUBOTA, T. (1984), "Visible structure of buoyant diffusion flames", Twentieth (International) Symposium on Combustion, The Combustion Institute.

25. ANTONIA, R.A., PRABHU, A. and STEPHENSON, S.E. (1975), "Conditionally sampled measurements in a heated turbulent jet", J. Fluid Mech., 72, 455.

26. BECKER, H.A., HOTTEL, H.C. and WILLIAMS, G.C. (1967), "The nozzle-fluid concentration field of the round, turbulent jet", J. Fluid Mech., 30, 285.

27. BIRCH, A.D., BROWN, D.R., DODSON, M.G. and THOMAS, J.R. (1978), "The turbulent concentration field of a methane jet", J. Fluid Mech., 88, 431.

28. LOCKWOOD, F.C. and MONEIB, H.A. (1980), "Fluctuating temperature measurements in a heated round jet", Comb. Sci. Tech., 22, 3.

29. NAKAMURA, I., SAKAI, Y. and MIYATA, M. (1982), "A study on the fluctuation concentration field in a turbulent jet", Nagoya Univ. Reports, 34, 113.

30. CHEVRAY R. and TUTU, N.K. (1978), "Intermittency and preferential transport of heat in a round jet", J. Fluid Mech., 88, 133.

31. CORRSIN, S. and UBEROI, M.S. (1950), "Further experiments on the flow and heat transfer in a heated turbulent jet", NACA Report 998.

32. BROADWELL, J.E. and BREIDENTHAL, R.E. (1982), "A simple model of mixing and chemical reaction in a turbulent shear layer", J. Fluid Mech., 125, 397.

33. UBEROI, M.S. and SINGH, P.I. (1975), "Turbulent mixing in a two-dimensional jet", Physics of Fluids, 18, 764.

END

1-87

DTIC